Cell Metabolism

Article

Microbiota alterations in proline metabolism impact depression

Graphical abstract

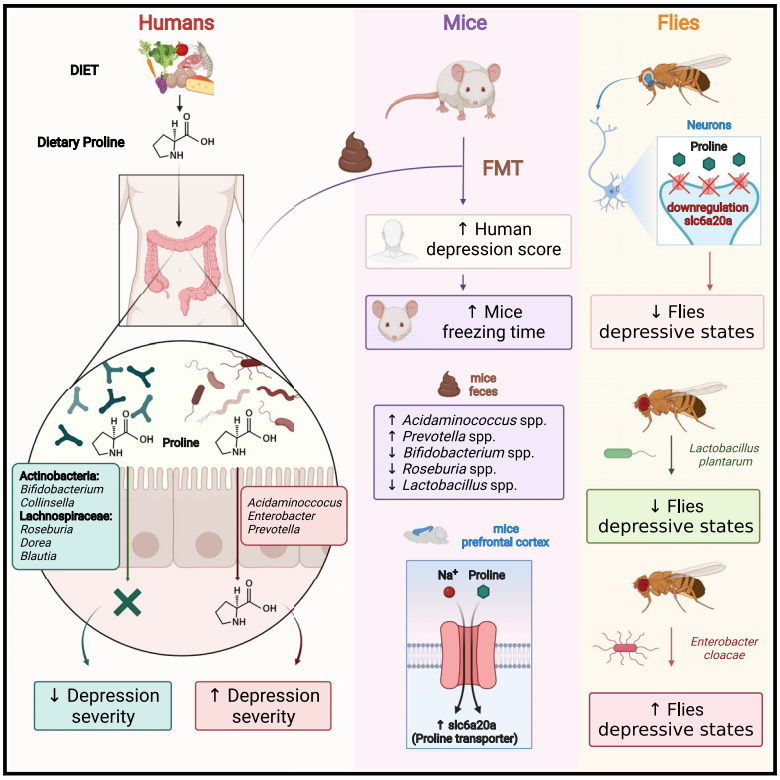

Highlights

- High dietary and plasma proline significantly associate with depression severity
- Circulating proline is dependent on microbiome composition and functionality
- With FMT, depression phenocopies to mice and increases a proline transporter gene
- *Slc6a20* knockdown and *L. plantarum* supplementation protect flies from depression

Authors

Jordi Mayneris-Perxachs, Anna Castells-Nobau, María Arnoriaga-Rodríguez, ..., Gustavo Deco, Rafael Maldonado, José Manuel Fernández-Real

Correspondence

jmayneris@idibgi.org (J.M.-P.), rafael.maldonado@upf.edu (R.M.), jmfreal@idibgi.org (J.M.F.-R.)

In brief

Mayneris-Perxachs et al. apply a multi-omics approach to study the microbiota-gut-brain axis in depression and demonstrate that microbiome-dependent elevations in plasma proline are significantly associated with depression severity in humans. Proline supplementation exacerbated depression in mice, and knockdown of proline and GABA transporters or mono-association with *L. plantarum* conferred protection against depression-like states in *Drosophila*.

Mayneris-Perxachs et al., 2022, Cell Metabolism *34*, 681–701
May 3, 2022
https://doi.org/10.1016/j.cmet.2022.04.001

CellPress

Cell Metabolism

CellPress
OPEN ACCESS

Article

Microbiota alterations in proline metabolism impact depression

Jordi Mayneris-Perxachs,[1,2,3,29,*] Anna Castells-Nobau,[1,2,3] María Arnoriaga-Rodríguez,[1,2,3,4] Miquel Martin,[5] Lisset de la Vega-Correa,[1,2,3] Cristina Zapata,[1,2,3] Aurelijus Burokas,[5,6] Gerard Blasco,[7,8] Clàudia Coll,[9] Anira Escrichs,[10] Carles Biarnés,[7,8,11] José María Moreno-Navarrete,[1,2,3,4] Josep Puig,[4,7,8,11] Josep Garre-Olmo,[12,13,14] Rafel Ramos,[4,15,16] Salvador Pedraza,[4,8,11] Ramón Brugada,[16,17] Joan Carles Vilanova,[11,16] Joaquín Serena,[16,18] Jordi Gich,[4,18]

(Author list continued on next page)

[1]Department of Diabetes, Endocrinology and Nutrition, Dr. Josep Trueta Hospital, Girona, Spain
[2]Girona Biomedical Research Institute (IDIBGI), Girona, Spain
[3]CIBER Fisiopatología de la Obesidad y Nutrición (CIBEROBN), Girona, Spain
[4]Department of Medical Sciences, School of Medicine, Girona, Spain
[5]Laboratory of Neuropharmacology, Department of Experimental and Health Sciences, Universitat Pompeu Fabra, Barcelona, Spain
[6]Institute of Biochemistry, Life Sciences Center, Vilnius University, Vilnius, Lithuania
[7]Institute of Diagnostic Imaging (IDI)-Research Unit (IDIR), Parc Sanitari Pere Virgili, Barcelona, Spain
[8]Medical Imaging, IDIBGI, Girona, Spain
[9]Girona Neuroimmunology and Multiple Sclerosis Unit, Department of Neurology, Dr. Josep Trueta Hospital, Girona, Spain
[10]Computational Neuroscience Group, Center for Brain and Cognition, Department of Information and Communication Technologies, Universitat Pompeu Fabra, Barcelona, Spain
[11]Department of Radiology (IDI), Dr. Josep Trueta Hospital, Girona, Spain
[12]Research Group on Aging, Disability, and Health, Girona Biomedical Research Institute (IdibGi), Girona, Spain
[13]Serra-Hunter Fellow, Department of Nursing, University of Girona, Girona, Spain
[14]Institut d'Assistència Sanitària, Girona, Spain
[15]Vascular Health Research Group of Girona (ISV-Girona), Jordi Gol Institute for Primary Care Research (Institut Universitari Recerca Atenció Primària Jordi Gol i Gorina-IDIAPJGol), Girona, Spain
[16]IDIBGI, Dr. Josep Trueta Hospital, Girona, Spain
[17]Biomedical Research Networking Center for Cardiovascular Diseases (CIBER), Madrid, Spain
[18]Girona Neurodegeneration and Neuroinflammation Group, IDIBGI, Girona, Spain
[19]Area of Genomics and Health, Foundation for the Promotion of Health and Biomedical Research of València Region (FISABIO-Public

(Affiliations continued on next page)

SUMMARY

The microbiota-gut-brain axis has emerged as a novel target in depression, a disorder with low treatment efficacy. However, the field is dominated by underpowered studies focusing on major depression not addressing microbiome functionality, compositional nature, or confounding factors. We applied a multi-omics approach combining pre-clinical models with three human cohorts including patients with mild depression. Microbial functions and metabolites converging onto glutamate/GABA metabolism, particularly proline, were linked to depression. High proline consumption was the dietary factor with the strongest impact on depression. Whole-brain dynamics revealed rich club network disruptions associated with depression and circulating proline. Proline supplementation in mice exacerbated depression along with microbial translocation. Human microbiota transplantation induced an emotionally impaired phenotype in mice and alterations in GABA-, proline-, and extracellular matrix-related prefrontal cortex genes. RNAi-mediated knockdown of proline and GABA transporters in *Drosophila* and mono-association with *L. plantarum*, a high GABA producer, conferred protection against depression-like states. Targeting the microbiome and dietary proline may open new windows for efficient depression treatment.

INTRODUCTION

Depression affects more than 300 million people worldwide and is well known to constitute one of the main causes of disability (James et al., 2018; WHO, 2020). The underlying mechanisms of depression remain a crucial unresolved research topic, evidenced by the lack of an appropriate treatment, an overall efficacy below 50% in those treated, and a relapse rate of 40% in responders (Hansen et al., 2008; Zhou et al., 2020). The benefits become clinically relevant only in the small minority of patient

Lluís Ramió-Torrentà,[4,9,18] Vicente Pérez-Brocal,[19,20] Andrés Moya,[19,20,21] Reinald Pamplona,[22] Joaquim Sol,[22,23,24] Mariona Jové,[22] Wifredo Ricart,[1,2,3,4] Manuel Portero-Otin,[22] Gustavo Deco,[10,25,26,27] Rafael Maldonado,[5,28,*] and José Manuel Fernández-Real[1,2,3,4,29,30,*]
Health), València, Spain
[20]Biomedical Research Networking Center for Epidemiology and Public Health (CIBEResp), Madrid, Spain
[21]Institute for Integrative Systems Biology (I2Sysbio), University of València and Spanish Research Council (CSIC), València, Spain
[22]Metabolic Physiopathology Research Group, Experimental Medicine Department, Lleida University-Lleida Biochemical Research Institute (UdL-IRBLleida), Lleida, Spain
[23]Institut Català de la Salut, Atenció Primària, Lleida, Spain
[24]Research Support Unit, Fundació Institut Universitari recerca l'Atenció Primària Salut Jordi Gol i Gorina (IDIAPJGol), Lleida, Spain
[25]Institucio Catalana de la Recerca i Estudis Avançats (ICREA), Barcelona, Spain
[26]Department of Neuropsychology, Max Planck Institute for human Cognitive and Brain Sciences, Leipzig, Germany
[27]Turner Institute for Brain and Mental Health, Monash University, Melbourne, VIC, Australia
[28]Hospital del Mar Medical Research Institute (IMIM), Barcelona, Spain
[29]These authors contributed equally
[30]Lead contact
*Correspondence: jmayneris@idibgi.org (J.M.-P.), rafael.maldonado@upf.edu (R.M.), jmfreal@idibgi.org (J.M.F.-R.)
https://doi.org/10.1016/j.cmet.2022.04.001

populations with severe major depression. Therefore, there is an urgent need for new insights into its pathophysiology.

A promising novel area of investigation involves the microbiota-gut-brain axis (Liang et al., 2018), recently shown to control cognitive function (Arnoriaga-Rodríguez et al., 2020) and inhibitory behavior (Arnoriaga-Rodríguez et al., 2021). The microbiome influences the gut-brain communication through endocrine, immune, and neuroactive pathways. The latter includes microbial-derived neurotransmitters (e.g., γ-aminobutyric acid [GABA] and catecholamines) and metabolites (short-chain fatty acids [SCFAs] and bile acids), as well as brain-derived neurotrophic factors (Cryan et al., 2019). A recent systematic review that identified 19 studies analyzing the gut microbiota in depression revealed largely inconsistent findings (Simpson et al., 2021) due to underpowered cross-sectional case-control studies focusing mainly on taxonomic composition based on 16S rRNA sequencing. It is mandatory to develop powerful longitudinal studies to clarify the specific role of microbiota in depression. Subjects with mild depression should also be investigated to evaluate the spectrum of depressive symptomatology and potentially provide preventive measures. In addition, different microbial signatures may result in the same phenotype due to functional redundancy. Going beyond taxonomic composition to include analyses of microbial functionality, metabolomics, and shotgun metagenomics sequencing is vital to accurately capture the host-microbiome interplay. Finally, with just two exceptions, the studies did not consider essential confounding variables known to influence depression or the gut microbiota composition, particularly diet (Wu et al., 2011) or psychotropic medication. Only one study applied appropriate statistical methods to take into account the compositional nature of the microbiome datasets.

RESULTS

Depression scores are associated with a specific microbial ecosystem

We applied an integrative longitudinal, multi-cohort, and multi-omics approach to reveal molecular mechanisms underlying the microbiome-gut-brain axis interplay in depression. We first assessed the relationships of bacterial composition and functionality with depression using the Patient Health Questionnaire 9 (PHQ-9) in a longitudinal discovery cohort (IRONMET, n = 116; Table S1A) comprising non-depressed (n = 44, PHQ-9: 0–4), mildly depressed (n = 47, PHQ-9: 5–9), and major depressed subjects (n = 25, PHQ-9: >10) (Kroenke et al., 2001).

With few exceptions (Stevens et al., 2021; Valles-Colomer et al., 2019), previous studies analyzing the associations between the gut microbiome and depression have not used compositional data analysis, rendering potential misleading conclusions. We modeled read counts using a Dirichlet distribution to deal with 0 count values and then applied a centered log-ratio (clr) transformation as implemented in the ALDEx2 R package (Gloor et al., 2017; Fernandes et al., 2014). Previous studies have reported inconsistent alpha diversity findings, and some reported lower indices in subjects with major depressive disorder (MDD) compared with controls (Simpson et al., 2021). In line with this, we did not observe significant differences in the alpha diversity measures such as species richness or the Shannon index among groups (Figure 1A). However, non-depressed individuals had higher Fisher's alpha diversity indices than depressed subjects. No differences were found between mild and major depression. The compositional alternative to the principal coordinate analysis plots of beta-diversity is the principal component analysis (PCA). We applied a PCA to the clr-transformed data to reveal global variance patterns in the microbial profiles and identified outliers. This initial unsupervised exploratory analysis revealed significant differences in the microbiome composition between non-depressed and depressed subjects (Figure 1B).

The vast majority of previous studies were based on 16S rRNA gene sequencing, and consequently, they do not provide enough taxonomic resolution to report results at the species level. For each taxa, we fitted a robust linear regression model between the PHQ-9 scores and the clr-transformed data controlling for age, sex, body mass index (BMI), education years, and antidepressant and anxiety medication. We were able to identify 30 bacterial species significantly associated with depression (p adjusted [padj] < 0.1) (Figure 1D; Table S2A). Patients with higher PHQ-9 scores had higher levels of *Parabacteroides spp.* and *Acidaminococcus spp.* but lower levels of *Bifidobacterium pseudolongum* and species from the butyrate-producing

CellPress
OPEN ACCESS

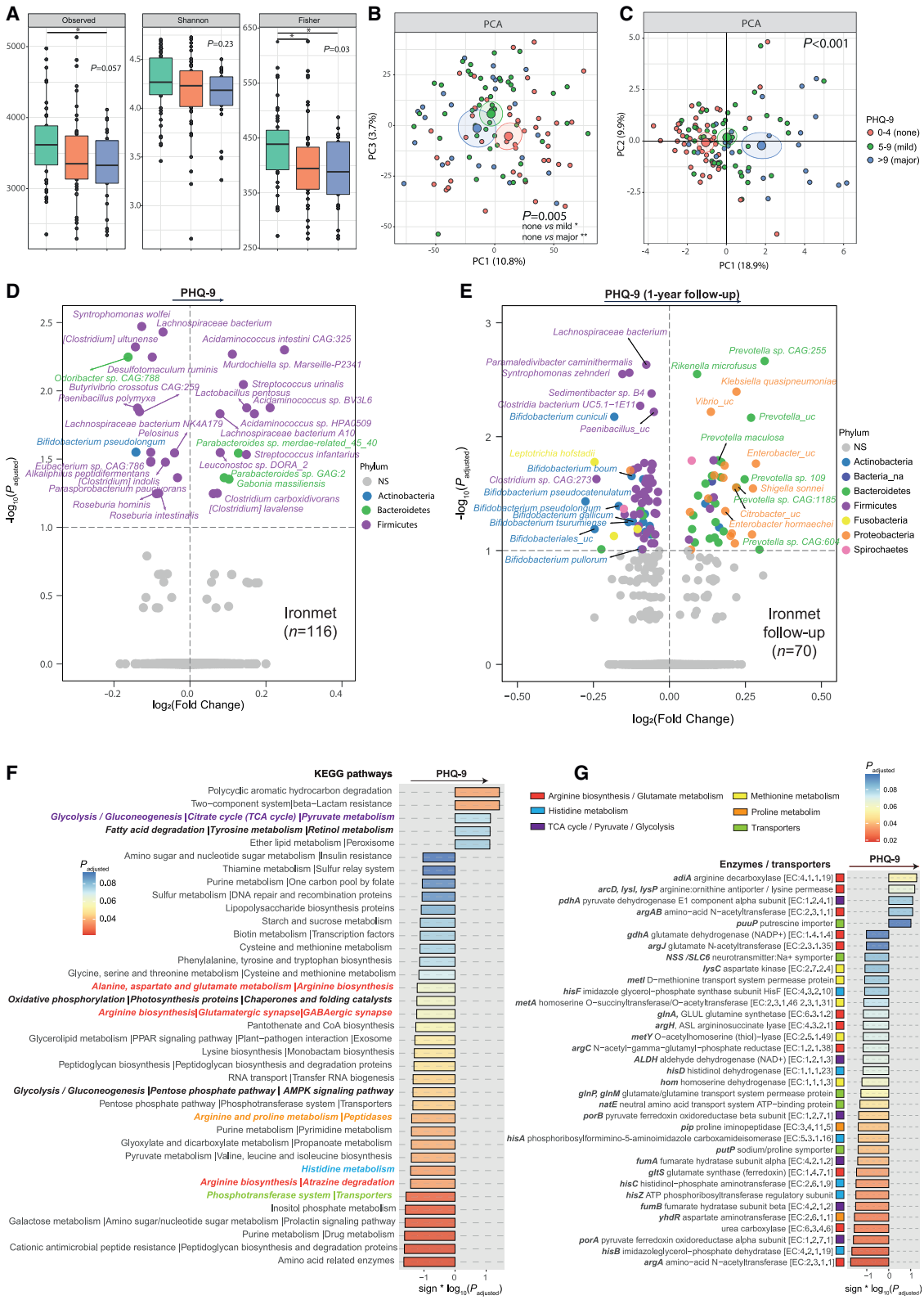

(legend on next page)

Lachnospiraceae family. All previous case-control studies were cross-sectional in nature. Longitudinal comparisons of baseline bacterial taxa predictive of the PHQ-9 score 1 year later disclosed lower levels of *Actinobacteria* (*Bifidobacterium spp.* and *Colinsella spp.*) and *Lachnospiraceae* species and higher levels of *Prevotella* and *Enterobacter* species associated with higher PHQ-9 scores 1 year later (Figure 1E; Table S2B).

Medication can influence the gut microbiota (Jacobs et al., 2017). A PCA on the clr-transformed data showed no difference in the microbial profiles between patients taking or not taking antidepressants (Figure S1A) or anxiolytics (Figure S1B), in line with a recent study that found no influence of antidepressant medication on taxa clustering by PCA (Stevens et al., 2021). We did not find any differential bacterial taxa between patients taking or not taking anxiolytics (Table S2C). A small number of taxa was associated with antidepressant use (Figure S1C; Table S2D). However, all of these bacterial species belonged to the Firmicutes phylum, mainly the *Clostridium* genera, and were not identified as associated with the PHQ-9 scores.

Gut dysbiosis triggers a pro-inflammatory state in the host by increasing the permeability of the gut barrier, facilitating the translocation of bacterial antigens into the circulation leading to low-grade inflammation (Maes et al., 2012). Increased intestinal barrier permeability has been associated with altered gut microbiota in anxiety or depression (Stevens et al., 2018). We measured serum lipopolysaccharide binding protein (LBP), a surrogate marker of bacterial translocation, and zonulin, the master regulator of intestinal permeability, by modulating intercellular tight junctions (Fasano, 2012). Gut dysbiosis has been shown to activate zonulin release (Asmar et al., 2002). In agreement with previous results, both biomarkers of gastrointestinal tract barrier integrity correlated positively with the PHQ-9 scores (LBP, $r = 0.23$, $p = 0.007$; zonulin, $r = 0.17$, $p = 0.04$).

Microbial functions linked to depression

Due to functional redundancy, significantly different microbial compositions may produce the same functional outcome (Mayneris-Perxachs and Fernández-Real, 2020). Different phylotypes can cover identical functions and produce the same metabolic outputs under the same environmental conditions. Reads originating from microbial genes were mapped to the Kyoto Encyclopedia of Genes and Genomes (KEGG) orthologs. Fitted generalized linear models to the clr-transformed KEGG counts, partialling out the effects of age, sex, BMI, education years, and antidepressants and anxiolytics medication, revealed several pathways (KEGG orthology level 3) associated with the PHQ-9 score (padj < 0.1) (Figure 1F). Bacterial pathways involving arginine, proline, and histidine metabolism were negatively associated with depression. Along with glutamine, their catabolism converges into glutamate, which serves as a carbon source for fueling the TCA cycle and subsequent gluconeogenic reactions, as well as the synthesis of GABA. Consistently, we also found significant associations of bacterial glutamate metabolism, glutamatergic synapse, and GABAergic synapse with the host PHQ-9 scores. Deeper analysis of the functional terms (KEGG orthology level 4) identified 327 out of 5,714 bacterial functions significantly associated with depression scores (Table S2E). Some of the bacterial functions with the strongest associations were involved in the TCA cycle (Figure 1G). Remarkably, the solute carrier family 6 (SLC6) also had a negative association with PHQ-9 scores. SLC6 genes mainly encode transporters for neurotransmitters (e.g., GABA, monoamines, glycine, and proline), but also proteinogenic amino acids, betaine, taurine, and creatine (Bröer and Gether, 2012), consistent with alterations in the GABAergic synapse. At the pathway level, we did not find any significant association among microbial pathways and anxiolytic (Table S3A) or antidepressant (Table S3B) use. At the functional term level, we found five and six bacterial functions associated with anxiolytic (Figure S1E; Table S3C) and antidepressant (Figure S1D; Table S3D) medication, respectively. None of these functions were associated with the PHQ-9 scores.

Metabolites from the histidine, arginine, and proline degradation pathways converging into glutamate and GABA shunt are associated with depression

To further explore the microbiome functionally, we next performed a metabolic profiling of plasma and fecal samples. Metabolic phenotyping provides a readout of the actual microbiota functional activity (Mayneris-Perxachs and Fernández-Real, 2020). Applying a machine learning variable selection strategy based on multiple random forest (Kursa and Rudnicki, 2010), we identified several metabolites linked to the PHQ-9 scores (Figures 2A–2D, S2A, and S2B). Consistent with previous findings, several of these metabolites were involved in the TCA cycle (succinate and fumarate), histidine metabolism (urocanate), and proline and glutamate metabolism. We validated these findings by performing an HPLC-MS/MS-based metabolic profiling of

Figure 1. Associations of the gut microbiota composition and functionality with depression cores

(A) Boxplots of alpha diversity indices (IRONMET, n = 116, Kruskal-Wallis).

(B) PCA score plot based on clr-transformed shotgun sequencing metagenomic microbial taxonomy data, colored according to depression status. Overall differences in the microbiome composition were assessed by PERMANOVA using 1,000 permutations and Euclidean distances. Pairwise differences between groups were assessed using the *pairwise.adonis* function adjusted for Bonferroni correction. *p < 0.05; **p < 0.01.

(C) PCA score plot based only on significant microbial species associated with the PHQ-9 scores.

(D and E) Volcano plots of differential bacteria associated with the baseline (D) and 1-year follow-up of PHQ-9 scores identified in the IRONMET cohort (E) after fitting a robust linear regression model to the clr-transformed data controlling for age, sex, BMI, education years, and antidepressant and anxiety medication. The $\log_2$ fold change associated with a unit change in the clr-transformed values and the $\log_{10}$ p values adjusted for multiple testing are plotted for each taxon. Significantly different taxa are colored according to phylum.

(F and G) Manhattan-like plot of significant KEGG bacterial pathways (F) and molecular functions (KEGG orthologs, KO) associated with the PHQ-9 scores identified from the clr-transformed shotgun metagenomics data in the IRONMET cohort controlling for age, sex, BMI, education years, and antidepressant and anxiety medication (G). Bars are colored according to the p value adjusted for multiple testing. The $-\log_{10}$(p adjusted) values are multiplied by the fold change sign to take into account the direction of the association. Pathways and functions involved in arginine, histidine, proline, methionine, glutamate, GABA, the TCA cycle, and related transporters are highlighted in color.

CellPress
OPEN ACCESS

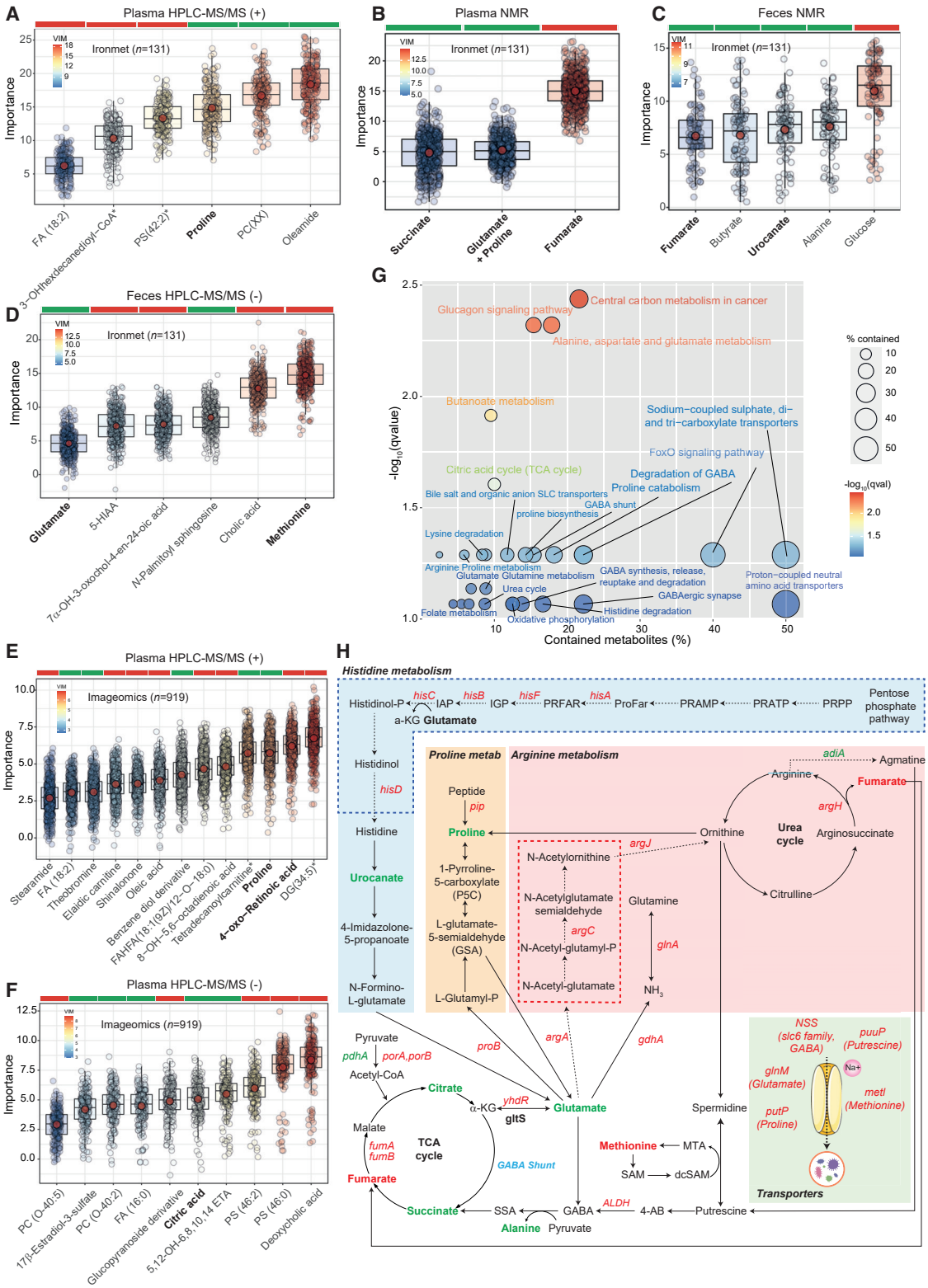

Figure 2. Plasma and fecal metabolites associated with the PHQ-9 depression scores in the IRONMET and IMAGEOMICS cohorts identified by machine learning

(A–D) Boxplots of the normalized variable importance measure (VIM) for the metabolites associated with the PHQ-9 scores in (A) plasma (HPLC-MS/MS in positive mode), (B) plasma (^{1}H-NMR), (C) feces (^{1}H-NMR), and (D) feces (HPLC-MS/MS in negative model) in the IRONMET (n = 131) cohort.

(legend continued on next page)

plasma samples in an independent large validation cohort (IMAGEOMICS, n = 919; Table S1B) consisting also of non-depressed, mild, and major depressed subjects. The most consistent finding was the strong positive association of circulating proline with the depression scores (Figures 2A and 2E). Other consistent findings implicated alterations in retinol metabolism (Figures 2E and S2B) and TCA cycle intermediates (citric acid; Figure 2F). To facilitate analysis and interpretation of these metabolomics results, we performed a pathway over-representation analysis mapping metabolites that were significantly associated with the PHQ-9 in the discovery cohort to the KEGG, Reactome, INOH, and HumanCyc databases included in the ConsensusPathDB (Kamburov et al., 2013). This enrichment analysis further highlighted a significant (q value [qval] < 0.1) over-representation of pathways associated with the TCA cycle and oxidative phosphorylation, glutamate metabolism, and arginine, proline, and histidine catabolism (Figure 2G). It also stressed a significant over-representation of SLC and amino acid transporters as well as the GABA synthesis/degradation pathway and its link with the TCA cycle through the GABA shunt, predominantly associated with neurotransmission in the mammalian brain. A summary of the main metabolites and bacterial functions associated with depression is shown in Figure 2H.

Plasma proline levels are dependent on the gut microbiome composition and functionality

Diet has a strong impact in modulating the composition and metabolic activity of the gut microbiome (Sonnenburg and Bäckhed, 2016). Therefore, we next evaluated the associations of macronutrients, vitamins, minerals, amino acids, and fatty acids derived from food-frequency questionnaires with the PHQ-9 scores in the IRONMET cohort. As dietary fibers can significantly alter the composition of the gut microbiome, we controlled the analyses for fiber intake in addition to the previous covariates. Strikingly, partial Spearman's rank correlation analysis revealed proline as the dietary factor with the strongest impact on depression (Figure 3A). Consistent with previous results, serum zonulin levels correlated positively with dietary proline consumption ($r = 0.18$, $p = 0.041$). The median proline consumption in the IRONMET cohort was 5.33 g/day (IQR: 4.33–6.71), which is close to the average proline daily intake of 5.2 g/day (World Health Organization, 2006). When subjects were categorized according to the median levels of plasma proline and dietary proline consumption, those with both dietary and plasma proline below the median (LPD-LPP, low proline diet-low proline plasma) had the lowest PHQ-9 scores, whereas individuals with both high dietary proline consumption and circulating proline above the median (HPD-HPP, high proline diet-high proline plasma) had the highest depression scores (Figure 3B). After correction for multiple testing, we did not find any significant association among any dietary item and the use of antidepressants (Table S4A) or anxiolytics (Table S4B).

As proline had the most consistent association with depression, with both plasma and dietary levels associated with depression in both the discovery and validation cohorts, we further analyzed the associations of proline with the gut microbiome. Remarkably, the circulating levels of proline were related to a microbial signature similar to that associated with the PHQ-9 scores. Plasma proline was positively associated with species from the *Parabacteroides* and *Prevotella* genera, but negatively with *Actinobacteria* (including *Bifidobacterium*) and SCFA-producing species from the *Lachnospiraceae* family such as the *Roseburia*, *Butyrivibrio, Dorea*, and *Blautia* genera (Figure 3C; Table S5A). Higher levels of *Parabacteroides* and *Acidaminococcus* species, but lower levels of species from the *Bifidobacterium* genera and *Lachnospiraceae* family, particularly *Roseburia spp*., were found in patients with plasma proline above the median (HPP), compared with those with plasma proline below the median (LPP) (Figure 3D).

We next questioned whether patients with LPP and HPP but high proline consumption had a different microbiota composition. Patients with higher proline consumption and higher plasma proline levels (HPD-HPP) had higher levels of *Parabacteroides* and *Acidaminococcus* species and lower levels of *Bifidobacterium* and SCFA-producing species, compared with patients with higher proline from the diet but lower plasma proline (HPD-LPP) (Figure 3E). In other words, patients who despite consuming high proline levels had low circulating proline levels had a microbiota composition consistent with that associated with lower depression scores. The microbiota of patients with a high consumption of proline but low circulating proline levels was also enriched in bacterial functions involved the transport and metabolism of proline. In addition, it was also associated with microbial genes associated with the PHQ-9 score such as those participating in the metabolism of other amino acids

(E and F) Barplots of VIM for the metabolites associated with the PHQ-9 score plasma samples from the IMAGEOMICS cohort (n = 919) identified by HPCL-ESI-MS/MS in positive (E) and negative modes (F). The red dot represents the mean, and the color bar above each plot indicates the sign of the association among the metabolites and the PHQ-9 scores, with red indicating negative correlation and green positive correlation. Significant metabolites were identified using a multiple random forest-based machine learning variable selection strategy as implemented in the Borutta algorithm with 5,000 trees and 500 iterations. All metabolites were identified based on exact mass, retention time, and MS/MS spectrum, except those (*) that were only identified based on exact mass and retention time.

(G) Pathway over-representation analysis of metabolites significantly associated with the PHQ-9 scores based on KEGG, Reactome, INOH, and HumanCyc databases. The bubble size represents the percentage of significant genes contained in each pathway. Bubbles are colored according to the p value adjusted for multiple testing (q values).

(H) Representation of the connections of histidine (blue), proline (orange), and arginine (red) metabolic pathways with the glutamate and GABA metabolism. It also shows how the GABA shunt interconnects the TCA cycle with GABA and glutamate. Dashed lines indicate pathways only occurring in bacteria. Metabolites and bacterial functions positively and negatively associated with the PHQ-9 scores are highlighted in green and red, respectively.

5-HIAA, 5-hydroxyindole acetic acid; benzene diol derivative, 3-methoxy-5-[7-methoxy-3-methyl-5-(prop-1-en-1-yl)-2,3-dihydro-1-benzofuran-2-yl]benzene-1,2-diol; bile alcohol 1, b-cholestane-3 a,7a,12a,23,25-pentol; chromanone derivative, 3-(3,7-dimethylocta-2,6-dien-1-yl)-5-hydroxy-8,8-dimethyl-2-(2,4,5-trihydroxyphenyl)-4H,8H-pyrano[3,2-g]chromen-4-one; EPA, eicosapentanoic acid, fatty acid; glycopyranoside derivative, 1,2,10-trihydroxydihydro-*trans*-linalyl oxide 7-O-b-D-glucopyranoside; PC, phosphatidylcholine; PIP, phosphatidylinositol phosphate; PS, phosphatidylserine.

CellPress
OPEN ACCESS

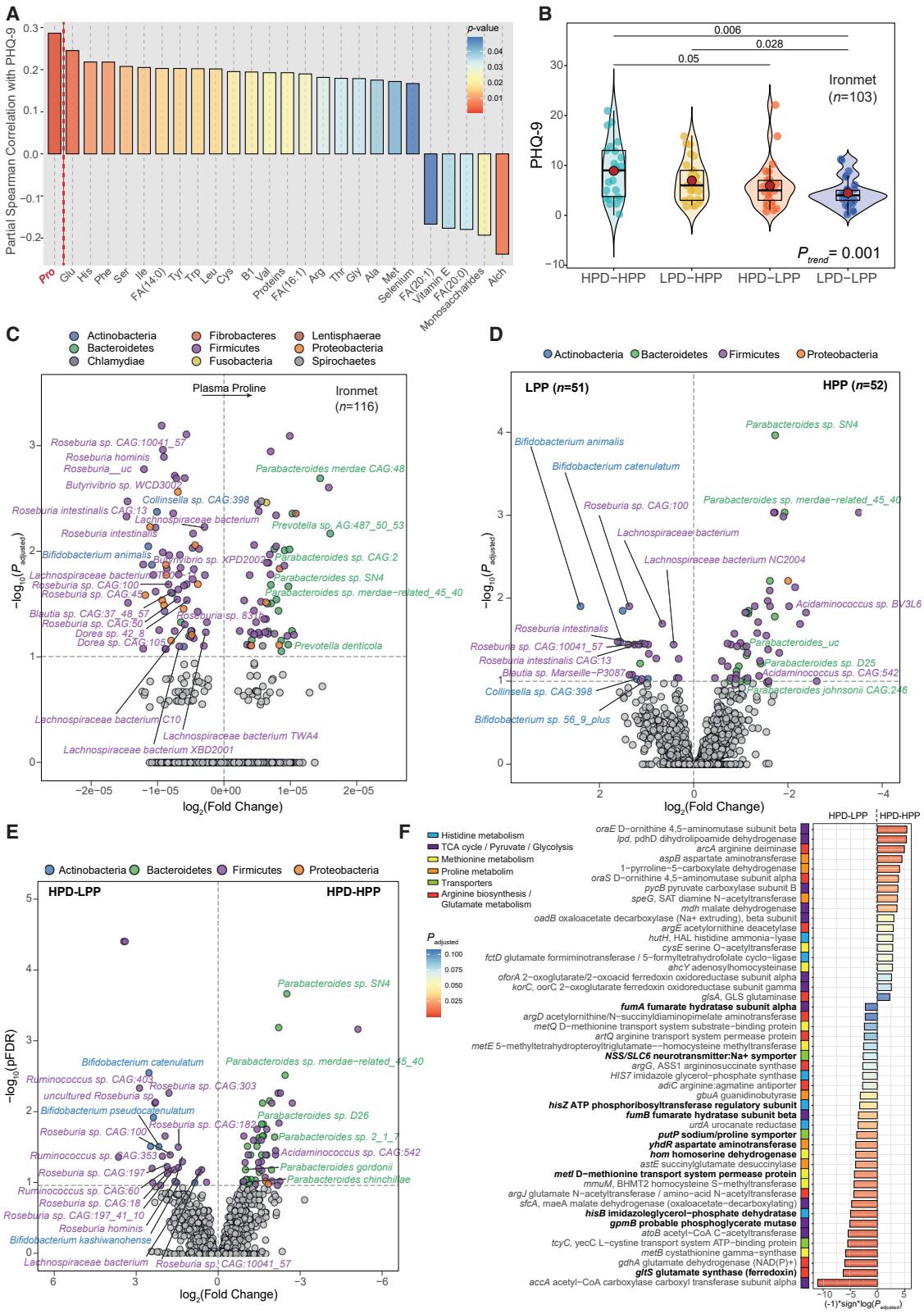

(legend on next page)

from the glutamate family, the TCA cycle, and the SLC6 family of transporters (Figure 3F; Table S5B).

High proline consumption is associated with small intestine genes participating in glutamatergic and GABAergic synapse and extracellular matrix homeostasis

As dietary proline is extensively metabolized by enterocytes in the small intestine (Figure 4A), we next performed RNA sequencing (RNA-seq) of jejunum samples from a second independent cohort (INTESTINE cohort, n = 28; Table S1C) to identify those transcripts associated with proline consumption. Differential gene expression analyses were performed following trimmed mean of M value (TMM) normalization using the limma pipeline with the *voom* transformation, linear modeling, and empirical Bayes moderation (Ritchie et al., 2015). We identified 1,547 out of 15,144 significant gene transcripts associated with dietary proline (Figure 4B; Table S6A). To facilitate functional interpretation of differentially expressed genes, we performed over-representation analyses mapping those genes to both Reactome (Figure 4C; Table S6B) and KEGG (Figure S3A; Table S6C) pathways. We collapsed redundant pathways into a single biological theme using enrichment map (Merico et al., 2010) to overcome redundancy and further simplify interpretation (Figures 4D and S3B). Reactome-based analyses identified pathways involved in GABA receptor activation, synaptic interactions, and axon guidance. It also revealed pathways participating in extracellular matrix (ECM), muscle contraction, MAPK signaling, and GPRC signaling. In line with these results, KEGG-based analyses highlighted several pathways involved in neuron synapse (Figures S3A and S3B), in particular GABAergic (Figure 3E) and glutamatergic synapse (Figure S3C), which is consistent with our metabolomics results. Our analyses in the jejunum also identified pathways participating in ECM and muscle contraction. We mapped significant transcripts associated with dietary proline to the DisGeNET disease-based database, which contains one of the largest collections of genes associated with human diseases, using both expert curated and text mining data. Enrichment analysis highlighted a significant over-representation of diseases associated with cognitive, neurodegenerative, and CNS disorders, including schizophrenia and MDDs (Figures S4A–S4C; Table S6D).

Proline supplementation exacerbates depressive-like behavior in mice in association with microbial translocation

To further investigate the direct effect of dietary proline on depression, we performed a supplementation study in mice (Figure 4F). A total of n = 20 CD-1 mice were fed a standard diet (SD) that was supplemented with either water or proline (36 g/L). Throughout the experiment, mice were chronically exposed to unpredictable mild stressors (unpredictable chronic mild stress [UCMS] model), an animal model with high face, and constant and predictive validity, to develop and evaluate depressive-like behavior. After 6 weeks of UCMS exposure, we did not find significant differences in either the body weight or drinking water among experimental groups. Mice supplemented with SD + proline had significantly higher circulating proline levels, compared with mice supplemented with the vehicle in both the control and UCMS groups (Figure S3D). They also had higher immobility times in the tail suspension test (Figure 4G), a well-validated model of the despair behavior, and reduced sucrose intake (Figure 4H), a behavioral model of anhedonia, a core symptom of depression, compared with stress-free control mice that only received water (SD + H_2O, n = 10). Additionally, compared with control animals, UCMS: SD + proline mice had higher levels of LBP (Figure 4I), which is indicative of microbial translocation and in agreement with our results in humans. Although there seems to be an increase in corticosterone levels after the UCMS exposure, particularly after proline supplementation, the differences were not significant (Figure S3E). This is in line with the previous literature. Indeed, repeated exposure to mild stress in mice usually leads to transitory changes in plasma corticosterone levels (Langgartner et al., 2020), and more sensitive and specific ad hoc tests are usually required to reveal possible changes in the regulation of the hypothalamo-pituitary-adrenal axis in mice exposed to UCMS (Surget et al., 2011).

Brain iron deposition and whole-brain functional dynamics reveal rich club network disruptions associated with both depression and circulating proline

Metagenomics, metabolomics, and RNA-seq analyses were consistent in identifying alterations in glutamatergic and GABAergic systems. Since iron plays a crucial role in glutamate

Figure 3. Associations of dietary and plasma proline with the PHQ-9 scores and the gut microbiota

(A) Partial Spearman's rank correlations of the depression scores with macronutrients, vitamins, minerals, amino acids, and fatty acids derived from food-frequency questionnaires controlling for age, BMI, sex, education years, kcal intake, antidepressant and anxiety medication, and fiber intake in the IRONMET cohort (n = 116). Items above the red dashed line are significant after adjusting for multiple comparisons (FDR).

(B) Violin plots of the PHQ-9 scores in the IRONMET cohort according to high or low proline levels in plasma (HPP or LPP, respectively) and high or low proline from the diet (HPD or LPD, respectively). Red dots represent the mean. Overall significance was assessed using a Mann-Kendall trend test and between-group significance using a Wilcoxon test.

(C) Volcano plots of differential bacteria associated with circulating proline levels identified in the IRONMET cohort after fitting a robust linear regression model to the clr-transformed data controlling for age, sex, BMI, education years, and antidepressant and anxiety medication.

(D) Volcano plots of differential bacteria for the comparison of patients with high plasma proline (HPP) versus low plasma proline (LPP) split based on the median plasma proline levels.

(E) Volcano plots of differential bacteria for the comparison of patients with high proline from the diet and high plasma proline levels (HPD-HPP) versus patients with high proline from the diet but low plasma proline levels (HPD-LPP) split based on the median values of dietary proline and plasma proline. The $\log_2$ fold change associated with a unit change in the clr-transformed values and the $\log_{10}$ p values adjusted for multiple testing are plotted for each taxon. Significantly different taxa are colored according to phylum.

(F) Manhattan-like plot of differentially expressed molecular functions (KEGG orthologs, KO) for the comparison HPD-HPP versus HPD-LPP identified from the clr-transformed shotgun metagenomics data in the IRONMET cohort controlling for age, sex, BMI, education years, and antidepressant and anxiety medication. Bars are colored according to the p value adjusted for multiple testing. The $-\log_{10}$(p adjusted) values are multiplied by the fold change sign to take into account the direction of the association. Functions also associated with the PHQ-9 scores are highlighted in bold.

CellPress
OPEN ACCESS

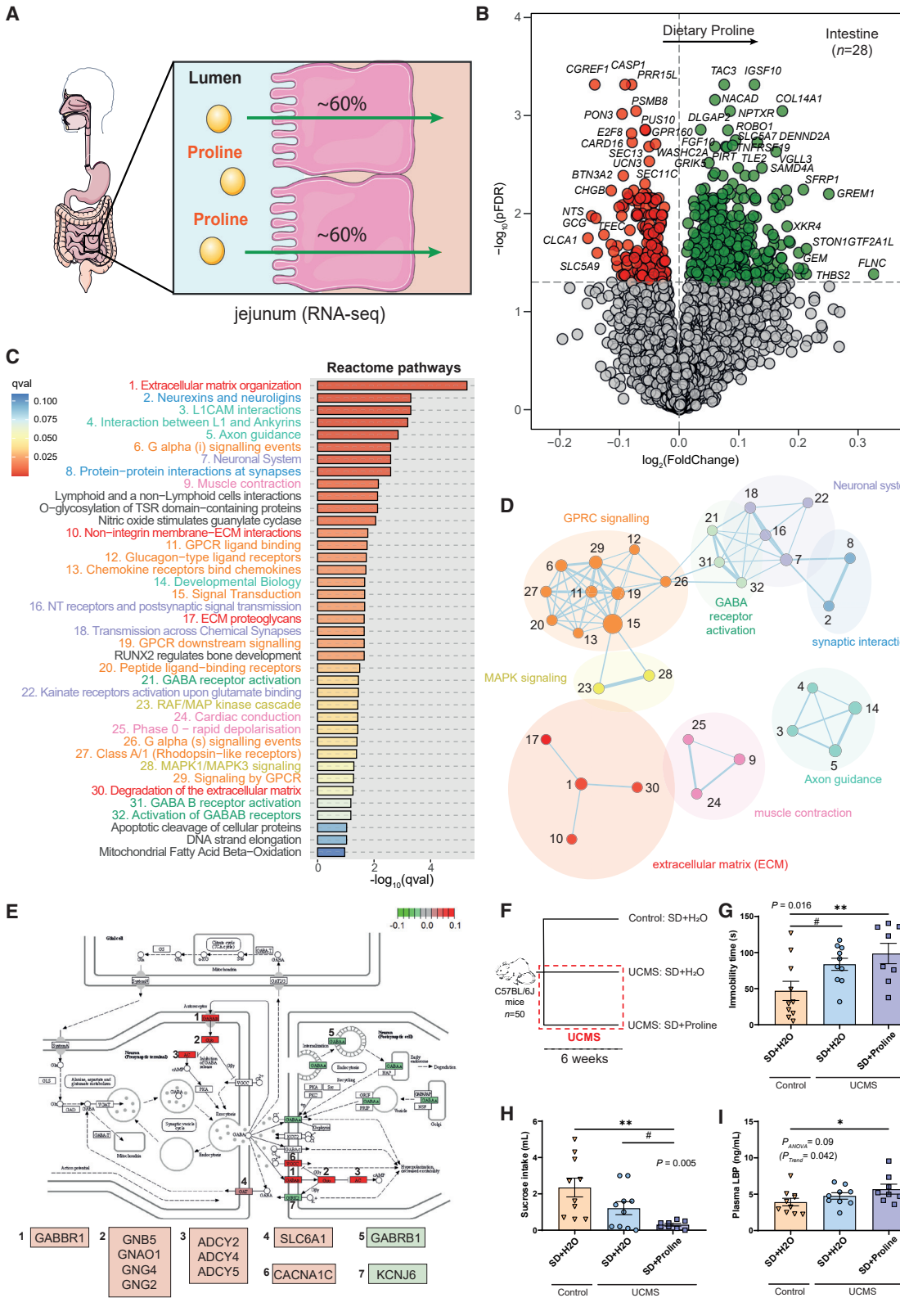

(legend on next page)

and GABA homeostasis, we assessed iron deposition in the brain of the IRONMET patients using magnetic resonance imaging (MRI) based on T2* and R2* relaxometry. In fact, iron overload in certain brain areas has been implicated in neurodegenerative disorders (Zecca et al., 2004) and alterations in anxiety-like behavior and mood (Kim and Wessling-Resnick, 2014), but only few studies have characterized the impact of iron on depression. It is also worth noting that the addition of proline to iron supplementation enhanced the number of red blood cells and hemoglobin, compared with administering iron alone (Kitajima et al., 2003). Partial Spearman's rank correlation analysis among relaxometry parameters in brain regions (AAL Atlas) and PHQ-9 scores highlighted low iron deposition (mean T2* values) of regions along the cingulum and frontal lobe positively associated with depression (Figure 5A). These results were validated using a machine learning variable selection strategy (Figure 5B). Moreover, the human brain is a complex network of structurally and functionally connected regions. Functional communication between these regions is thought to play a vital role in complex processes such as depression. However, most studies have focused on static functional connectivity, but functional connectivity among brain networks does not remain static over time. Studying the dynamics of resting-state brain activity across the whole-brain functional network might facilitate interpretation of brain functioning and provide better insights into the pathophysiology of disease (Escrichs et al., 2021). Therefore, we analyzed resting-state fMRI data (Figure 5C) in a subset of patients from the IMAGEOMICS cohort (n = 591) and studied whole-brain functional dynamics applying a novel intrinsic-ignition framework across the whole-brain functional network (214 brain areas) (Deco and Kringelbach, 2017) to assess the effect of spontaneous local activation events on local-global integration (Figure 5D), followed by machine learning algorithms to identify those nodes predictive of the PHQ-9 scores. Using the Boruta algorithm we identified 72 intrinsic-ignition nodes associated with depression (Figure 5E). Similarly, it revealed 68 nodes linked to the circulating proline levels (Figure 5F), 30 of which were also associated with the PHQ-9 scores (Figure 5G; Table S7). Notably, these shared intrinsic-ignition areas—including the superior frontal cortex, the precuneus, insula, and subcortical areas such as the caudate, putamen, and hippocampus—mostly belonging to the so-called rich club (Figure 5H), a set of high-degree nodes that tend to be more closely connected among themselves than with peripheral regions, i.e., lower degree nodes (Kim and Min, 2020; Puig et al., 2020).

An emotional impairment is transferred to mice through the gut microbiota: Direct impact on the expression of mPFC genes participating in proline and GABA transport and ECM and collagen metabolism in recipient mice

Finally, to evaluate a potential causal role of the microbiota in the development of emotional disorders, we transplanted microbiota from 20 human donors with different PHQ-9 scores into 20 antibiotic-treated mice (Figure 6A). Here, 11 donors had plasma proline levels below the median levels of the IRONMET cohort, whereas 9 donors had proline plasma levels above the median. The circulating plasma levels of the 20 donors were consistently positively associated with the PHQ-9 score (Figure S5A). In line with our previous results, the circulating proline levels of the donors were also positively associated with species from the *Parabacteroides*, *Acidaminococcus*, and *Prevotella* genera, but negatively with several species from the *Bifidobacterium* genera and SCFA-producing bacteria from the *Lachnosphiraceae* family (Figure S5B; Table S8A). To confirm engraftment, we analyzed the recipient mice microbiota using shotgun metagenomics sequencing. After fecal microbiome transplantation (FMT), 1,328 out of 1,926 taxa (~70%) from the donor's microbiota were also present in the recipient mice microbiota, indicating a favorable engraftment (Figure S5C). Notably, 184 from these 1,328 taxa were found in the microbiota of mice receiving FMT, but not in the microbiota of control mice receiving only antibiotics. A PCA of the clr-transformed data clearly showed a difference between the microbiota of control and FMT mice (Figure S5D).

We then assessed whether an emotionally impaired phenotype emerged in mice receiving microbiota from donors with higher depression scores using a fear conditioning-induced freezing test, a well-recognized model of maladaptive response to stress. Notably, donor's PHQ-9 scores were significantly correlated with the freezing time in recipient mice (Figure 6B). Consistently, the human donor's PHQ-9 score was associated

Figure 4. Associations of dietary proline with jejunal RNA sequencing

(A) Dietary proline is extensively metabolized by enterocytes in the small intestine (~40%).

(B) Volcano plot of differentially expressed jejunal gene transcripts associated with the consumption of proline identified by limma-voom controlling for age, BMI, sex, education years, kcal intake, and antidepressant medication (pFDR < 0.05) in the intestine cohort (n = 28).

(C) Pathway over-representation analysis of the jejunal genes significantly associated with the dietary proline based on Reactome database (qval < 0.1). Bars are colored according to the qval, and pathway names are colored based on the results of functional enrichment map so that pathways with the same color belong to the same cluster.

(D) Over-representation results were mapped as a functional network of clustered pathways using cytoscape and enrichment map. Nodes represent over-represented pathways. Node size reflects the total number of genes in each pathway. Edge thickness represents the degree of overlapping genes between pathways. Groups of functionally related pathways are circled and labeled. Pathways (nodes) are colored according to the functional group (cluster) to which they belong and are numbered according to (C). Nodes without overlap are not represented.

(E) KEGG map of regulation of the GABAergic synapse pathway, with each block representing a group of genes. A white block indicates that no gene in that block was significantly associated with dietary proline, whereas green/red backgrounds indicate significantly downregulated/upregulated genes, respectively. Node color reflects $\log_2$ fold change range. Over-expressed genes in each block are highlighted in the boxes below. Data were integrated and visualized using Pathview.

(F) Scheme of the proline supplementation study design. SD, standard diet; UCMS, unpredictable chronic mild stress.

(G–I) Immobility time (measured by tail suspension) (G), sucrose intake (H), and plasma lipopolysaccharide binding protein (LBP) (I) in the experimental groups. Results show the mean and bars represent SEM. Differences were assessed by one-way ANOVA followed by Tukey's or Dunnett's post hoc test in case of equal or different variances, respectively. A Mann-Kendal trend test was also used to analyze the linear trend in the plasma LBP measure.

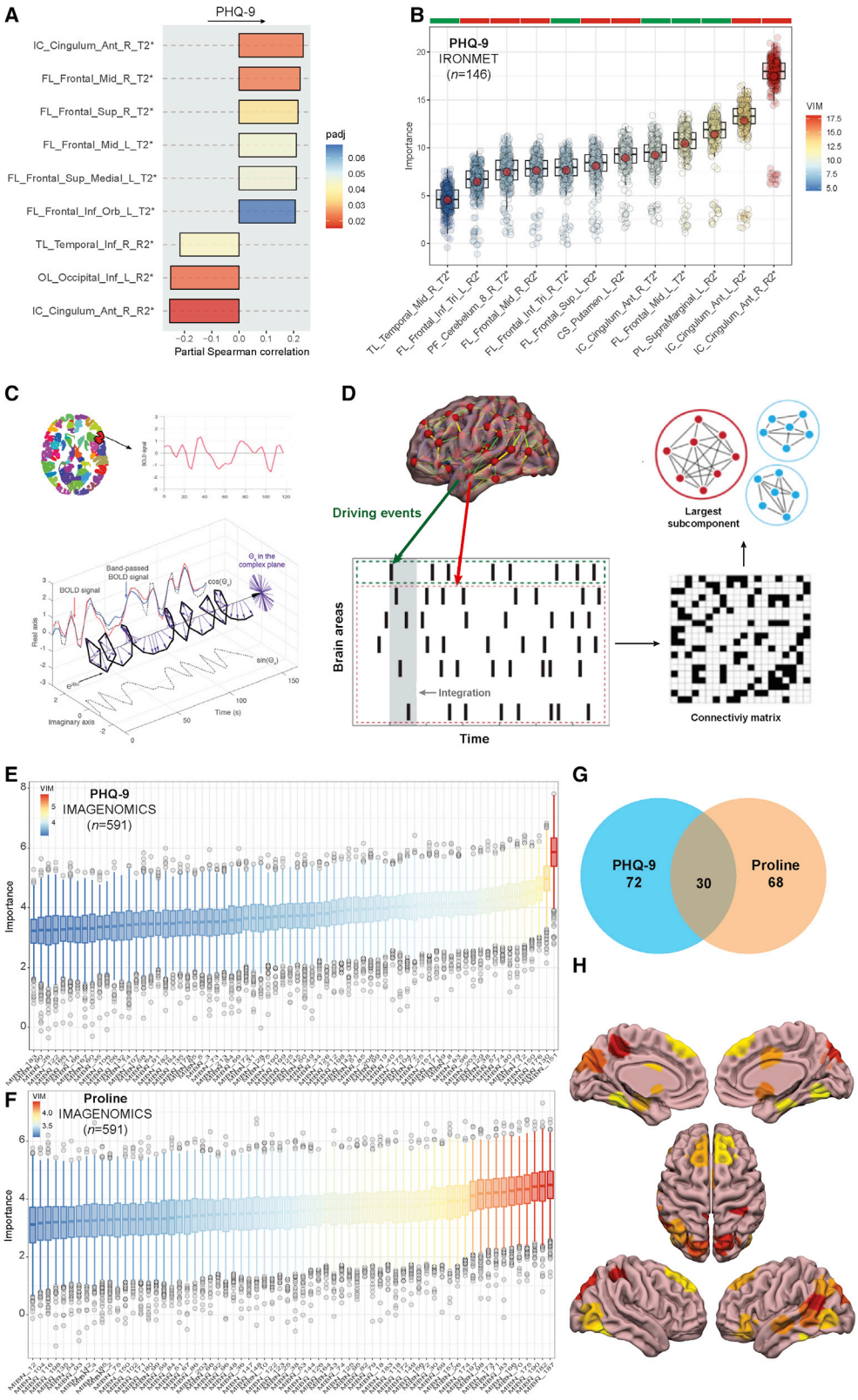

(legend on next page)

with a recipient mice microbiome signature very similar to that related to depression in humans, with positive associations with species from the *Acidaminococcus* and *Prevotella* genera and negative associations with species from the Actinobacteria phylum (particularly *Bifidobacterium spp.* and *Collinsella spp.*) and the SCFA-producing *Lachnospiraceae* family (Figure 6C; Table S8B). Not only was the donor's depression score associated with this bacterial signature, but also the recipient mice freezing time. Therefore, higher levels of *Prevotella* and *Parabacteroides* species in the mice microbiota were positively associated with the recipient mice freezing time, whereas *Bifidobacterium longum* and *Lachnospiraceae* species were negatively associated (Figure S5E; Table S8C).

One of the most consistent findings in MDD include decreased frontal lobe function, mainly involving the medial prefrontal cortex (mPFC) (Wang et al., 2012). In addition, results from a recent meta-analysis suggested that decreased levels of glutamatergic metabolites in the mPFC are linked with the pathophysiology of depression (Moriguchi et al., 2019). Considering our findings highlighting the impact of the microbiome on glutamatergic and GABAergic systems, we also performed RNA-seq of the mPFC of recipient mice. We identified 59 out of 15,537 gene transcripts in the recipient mice mPFC significantly associated with donor's PHQ-9 scores (Figures 6D and S5G; Table S8D). Notably, 44 (75%) of these gene transcripts were also associated with the recipient mice freezing time, including *slc6a12*, *slc6a13*, and *slc6a20a* (Figure S5F; Table S8E).

To gain better insight into the potential mechanisms underlying the microbial effects on depression, we built gene-gene interaction networks using the search tool for the retrieval of interacting genes/proteins (STRING) database (Szklarczyk et al., 2019; Figure 6E). Furthermore, we mapped significant genes to KEGG (Figure S5H) and Reactome (Figure 6F) databases. Half of the transcripts negatively associated with the donor's PHQ-9 score clustered together and were involved in oxidative phosphorylation and neurodegenerative disease. Notably, we identified a cluster comprising gene transcripts encoding for transporters of GABA (*slc6a12* and *slc6a13*) and proline (*slc6a20*) (Figure 6G), which is in agreement with our functional analyses. Consequently, we found an over-representation of Reactome pathways associated with GABA neurotransmission, which is also in consonance with the results from the jejunal RNA-seq analysis. These results are in line with metagenomics and metabolomics and highlight again the importance of the GABA shunt interconnecting the TCA cycle with GABA and glutamate metabolism. Not only that, but we also found another cluster of gene transcripts participating in ECM and collagen homeostasis and muscle contraction. Importantly, proline is essential for collagen biosynthesis, constituting 10% of its amino acid content. Therefore, these results validate and further highlight the importance of the proline-glutamate-GABA-microbiome interplay identified in our metabolomics and metagenomics analyses.

To further assess the potential causal role of the gut microbiota on the expression of gene transcripts in the mPFC, we integrated the recipient mice microbiota ("X") and transcriptome ("Y") associated with the donor's PHQ-9 scores using a partial least squares (PLS) model in regression model, which models the unidirectional (predictive or "causal," X → Y) relationship of "X" on "Y." Remarkably, we found that *Acidaminococcus spp.* had a strong predictive effect on the expression levels of those transcripts positively associated with higher donor's PHQ-9 scores, whereas *Bifidobacterium* species clustered with those transcripts associated with lower donor's depression scores (Figure 6H). Several species from the *Lactobacillus* genera were also close to this later cluster.

A decrease in the expression of proline and GABA transporters in neuronal and glial cells, respectively, confers protection against depression-like states in *Drosophila*

RNA-seq analysis of mouse prefrontal cortex revealed that the expression of proline (*Slc6a20*) and GABA transporters (*Slc6a12* and *Slc6a13*) was positively correlated with donor's PHQ-9 scores and mice freezing time after FMT (Figures 6D, 6G, and S5F). To further explore the role of these brain transporters in depression, we next used the model organism *Drosophila melanogaster*. To establish *Drosophila* models for stress-induced mood disorders, we submitted flies to repetitive episodes of mechanical stress for 12 h a day during a period of 5 consecutive days (STAR Methods). After that, we assessed flies' motivational state with (1) the GAP-climbing assay, measuring the

Figure 5. Associations of brain iron deposition and intrinsic brain networks with depression scores and circulating proline identified using machine learning

(A) Partial Spearman's rank correlations of the PHQ-9 scores with relaxometry parameters (mean R2* and T2* values) of brain regions from the anatomical automatic labeling brain atlas controlling for age, BMI, sex, education years, and antidepressant and anxiety medications in the IRONMET cohort (n = 146).

(B) Boxplots of the normalized variable importance measure (VIM) for the relaxometry measures of brain regions associated with the PHQ-9 scores. Red dots represent the mean.

(C) We extracted the BOLD time series using a resting-state atlas and computed the phase space of the BOLD signal for each brain area by using the Hilbert transform. The phase dynamics can be represented in the complex plane as $e^{i\varphi}$ (black bold line), the real part as cos(φ) (black dotted line), and the imaginary part as sin(φ) (black dotted line). The purple arrows represent the Hilbert phases at each TR. Adapted from Escrichs et al. (2021).

(D) Intrinsic-ignition framework. Events were obtained by applying a threshold method, and for each driving event, the activity in the rest of the network (see red stippled area) was obtained in the set 4TR time window (gray area). A binarized phase matrix was extracted from the time window. From this phase matrix, we obtained the integration by calculating the largest subcomponent and computed the mean ignition for each brain area across time. Adapted from .Escrichs et al. (2021).

(E and F) Boxplots of VIM for the mean ignition of brain areas associated with the PHQ-9 scores (E) and circulating proline in the IMAGENOMICS cohort (n = 591) (F). Significant variables in the machine learning analyses were identified using a multiple random forest-based variable selection strategy as implemented in the Borutta algorithm with 5,000 trees and 500 iterations.

(G) Venn diagram for the associations of the PHQ-9 and circulating proline.

(H) Some of these brain areas common to the circulating proline and PHQ-9 scores such as the superior frontal cortex, the precuneus, insula, and subcortical (i.e., the caudate, putamen, and hippocampus) belong to the so-called rich club.

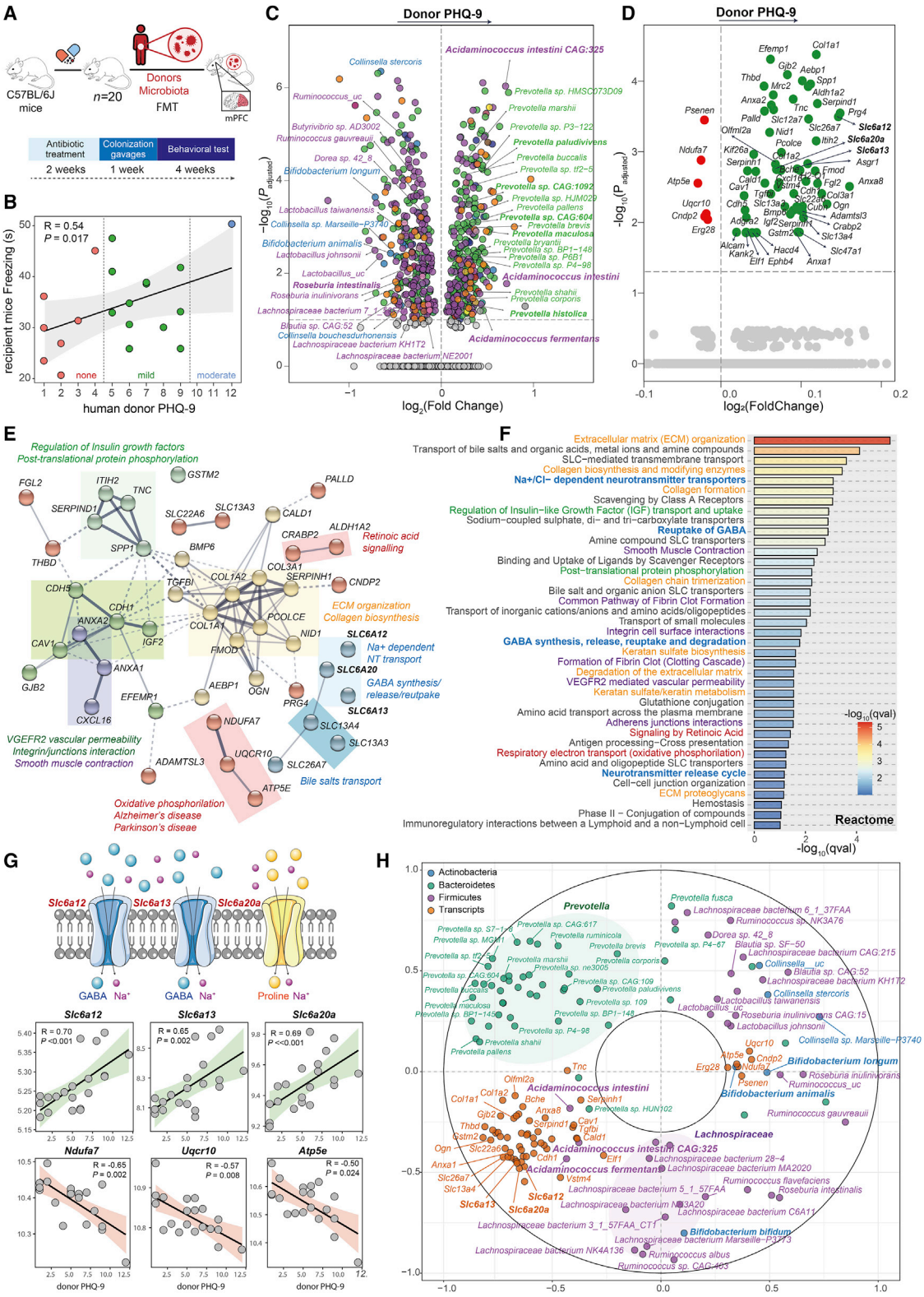

Figure 6. An emotionally impaired phenotype was phenocopied to recipient mice in parallel to changes in the expression of mPFC gene transcripts

(A) Experimental design for the FMT study. Microbiota from n = 20 human donors with different PHQ-9 scores was delivered to n =20 recipient mice pre-treated with antibiotics for 14 days. A freezing test was performed after 4 weeks.

(legend continued on next page)

motivation to climb an insurmountable 4.5-mm-wide gap by scoring the fly's typical leg-over-head behavior (Pick and Strauss, 2005); (2) the stop-for-sweet paradigm, which quantifies the number of times a starved fly stops to eat at a stripe of sweet tasting glycerol when performing negative geotaxis, measuring lack of appetite (Ries et al., 2017); and (3) the spontaneous locomotor activity, quantifying the total distance walked and the velocity while in motion for 5 min. Stress-treated control flies from all tested genotypes showed a significant reduction in GAP-climbing attempts, stooped less often to eat at the sweet tasting stripe, and reduced their total walking distance and velocity while in motion, compared with unstressed flies (Figures 7A–7G), showing a reduction of voluntary behavioral activity and overall lack of motivation, which are common symptoms of depression-like states (Ries et al., 2017).

We downregulated *CG43066*, the *Drosophila* ortholog of proline transporter *slc6a20*, via RNAi-mediated knockdown in neuronal cells with *Slc6a20-RNAi1*. We did not observe differences in GAP-climbing motivation (Figure 7A) or reduction of general locomotor activity (Figures 7C and 7D) between stressed and unstressed flies. The percentage of stops at the sweet tasting stripe was not different between stressed and unstressed groups in the stop-for-sweet paradigm; nonetheless, both groups stopped significantly less at the sucrose line than control unstressed flies (Figure 7B), and we suspected that these differences were due to a resistance to starvation. Therefore, we increased the starvation period of *Slc6a20-RNAi1* to 40 and 60 h. As expected, the number of stops at the sucrose line increased in a similar proportion in both groups, indicating that stress treatment did not reduce appetite between stressed and unstressed flies (Figure S6A). To confirm our results, we used a second RNAi line (*Slc6a20-RNAi2*); after pan-neuronal down regulation, a significant reduction in total walking distance was observed but not a decrease in velocity while in motion between stressed and unstressed flies (Figures 7G and 7H). No differences in GAP-climbing motivation or loss of appetite were observed in the GAP and stop or sweet paradigms (Figures 7E and 7F), resembling the results obtained with *Slc6a20-RNAi1*. Overall, these results indicate that low expression of the proline transporter in neurons confers resistance against depression states induced by mechanical stress in *Drosophila*.

We performed a pan-glial RNAi-mediated knockdown of *Drosophila* GABA transporter *Gat*, the ortholog of *Slc6a12* and *Slc6a13*, which is mainly expressed in glial cells. Although GAP-climbing motivation decreased in stressed flies (Figure 7I), we did not detect a reduction in percent of stops in the stop-for-sweet paradigm (Figure 7J), and flies were not reducing their general locomotor activity (Figures 7K and 7L) after stress treatment, indicating that downregulation of *Gat* in glial cell confers protection against depression-like states in mechanically stressed flies.

Mono-colonization with *L. plantarum* confers protection against depression-like states in *Drosophila*

Finally, to strengthen the causal effect of the microbiota on depression and our hypothesis about the importance of microbial production of GABA, we also used *Drosophila*. This model organism is easy to maintain in axenic conditions to generate mono-associated animals with wild-type microbiota species that are high or low GABA producers. Ideally, we would have selected *Acidaminococcus* and *Bifidobacterium*, as they had the most consistent opposite results in relation to depression both in humans and the FMT experiment. However, neither of the two genera are members of the *Drosophila* microbiota, as it is relatively simple (1–30 taxa), compared with the complex diversity associated with vertebrates (>500 taxa) (Broderick and Lemaitre, 2012). Thus, we selected 2 microbial species previously reported to be part of *Drosophila* microbiome (Broderick and Lemaitre, 2012) that we also found inversely associated with depression: *Lactobacillus plantarum* as high GABA producer and *Enterobacter cloacae* as a low GABA-producing species (Cui et al., 2020; Strandwitz, 2018). *Lactobacillus* species clustered close to the *Bifidobacterium* in the FMT study (Figure 6H), whereas *Enterobacter* species were positively associated with the PHQ-9 scores in humans (Figure 1E).

After *Drosophila* mono-association at the adult (Figure 7M) or larval stages (Figure S6D), a significant decrease in climbing motivation was observed in axenic and mono-colonized *E. cloacae* male, but not in *L. plantarum* mono-colonized male (Figures 7N and S6E). Similarly, female mono-colonized with *L. plantarum* did not show lack of appetite in the stop-for-sweet paradigm after stress treatment, although lack of appetite was

(B) Scatterplot and correlation between the donor's PHQ-9 scores and the recipient mice freezing test scores controlling for donor's age, BMI, sex, education years, and antidepressant and anxiety medication.
(C) Volcano plots of recipient mice differential bacteria associated with the human donor's PHQ-9 score after fitting a robust linear regression model to the clr-transformed data controlling for donor's age, sex, BMI, education years, and antidepressant and anxiety medication.
(D) Volcano plot of differentially expressed gene transcripts in the medial prefrontal cortex of the recipient mice associated with the donor's PHQ-9 scores identified by both limma-voom and DESeq2 after adjusting p values for multiple testing (padj). Genes involved in GABA (*slc6a12* and *slc6a13*) and proline (*slc6a20a*) transport are highlighted in bold.
(E) Gene interaction network constructed using differentially expressed mPFC gene transcripts associated with donor's PHQ-9 via the search tool for the retrieval of interacting genes/proteins (STRING) database. The network nodes are genes and the edges represent the predicted functional interactions. The thickness indicates the degree of confidence prediction of the interaction. Functional gene clusters are colored and annotated based on pathway over-representation analysis results.
(F) Reactome-based pathway over-representation analysis of the recipient's mice genes significantly associated with the donor's PHQ-9 scores (qval < 0.1). Bars are colored according to the qval, and pathway names are colored based on the functional clusters identified with STRING.
(G) Scatterplots and correlations of gene transcripts encoding for GABA and proline transporters as well as those involved in oxidative phosphorylation.
(H) Correlation circle plot for the integration of the recipient mice microbiota and mPFC gene transcripts associated with the human donor's PHQ-9 score using a PLS model in regression mode (X [microbiome] → Y [transcripts]). Strongly positively associated variables or groups of variables are projected close to one another on the correlation circle (<0° angle). The variables or groups of variables strongly negatively associated are projected diametrically opposite (<180° angle) on the correlation circle. Variables not correlated are situated <90° from one another.

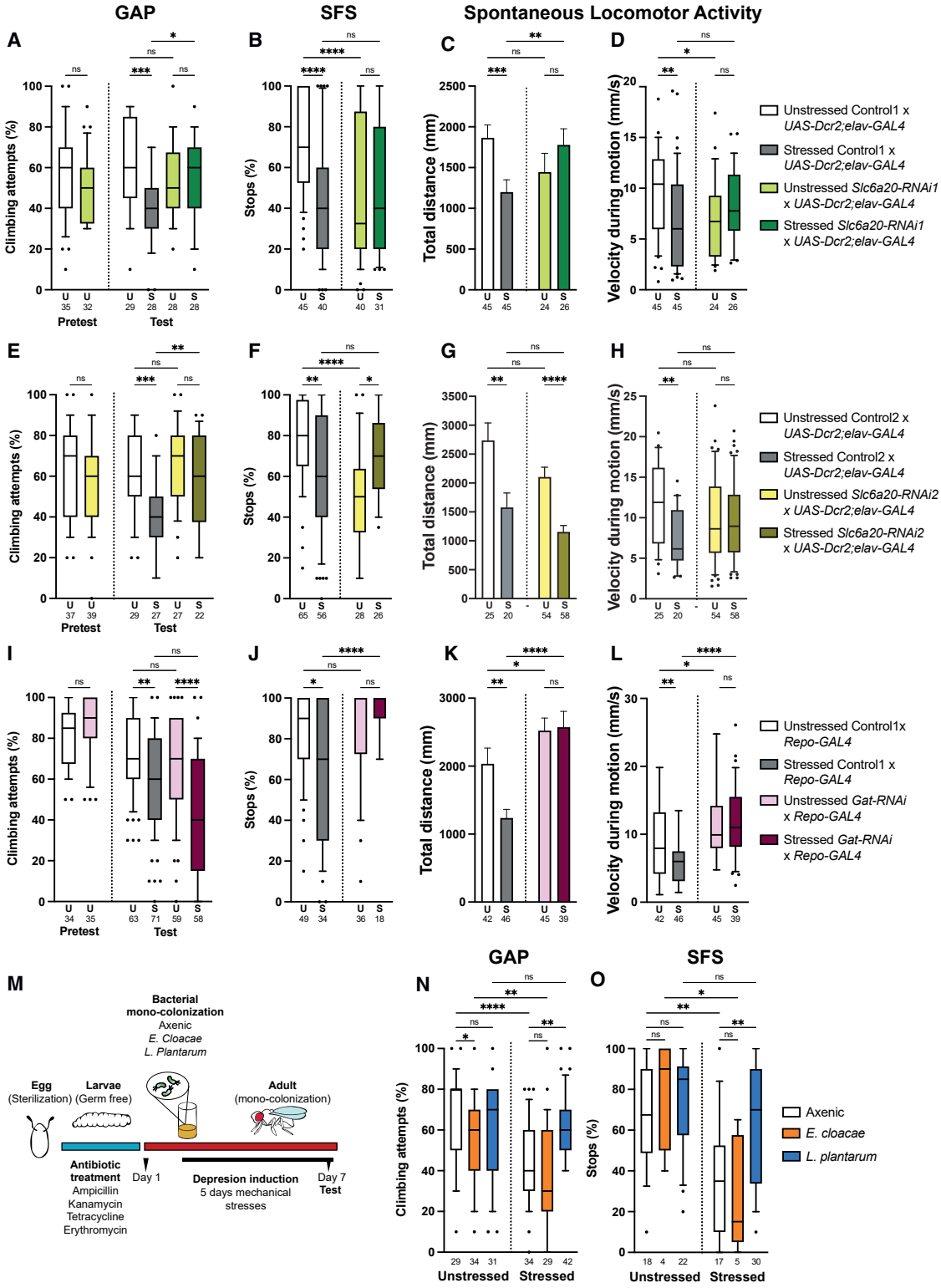

Figure 7. Pan-neuronal *Slc6a20* and pan-Glial *Gat* RNAi-mediated knockdown and mono-colonization of flies with *L. plantarum* showed protection against depression-like states in *Drosophila* after mechanical stress treatment

(A, E, and I) GAP-climbing assay. Males' motivation to climb an insurmountable 4.5-mm-wide gap. A significant decrease in climbing attempts was observed after 5 days of mechanical stress treatment in control flies, but not in unstressed males for all tested genotypes.

(A and E) Pan-neuronal downregulation of *Slc6a20* with RNAi1 and RNAi2 did not lead to significant differences in climbing attempts in males after stress treatment.

(legend continued on next page)

induced in axenic and mono-colonized *E. cloacae* stressed female (Figures 7O and S6F). *L. plantarum* or *E. cloacae* mono-associations did not prevent overall loss of locomotor activity when flies were mono-colonized at the adult stage (Figures 6G and 6H). Unstressed *L. plantarum* or *E. cloacae* mono-associated flies at larval stage walked less compared with unstressed axenic female, but no differences were observed between the stressed and unstressed groups. Velocity while in motion was not reduced between unstressed and stressed *L. plantarum* groups but was reduced in axenic and *E. cloacae* mono-colonized when flies were mono-associated at larval stage (Figures S6G and S6H) Overall, these results suggest that high GABA-producing bacteria like *L. plantarum* confer protection against depression-like states in the GAP-climbing assay and stop-for-sweet paradigm.

DISCUSSION

The gut microbiota has emerged as a novel actor in the pathophysiology of depression. However, recent meta-analyses have revealed a strong inconsistency among studies in terms of gut microbiome signatures associated with depression (Simpson et al., 2021). These inconsistencies mostly arise from underpowered studies, methodological heterogeneity, varying depression diagnostic criteria, lack of consideration of confounding variables, inappropriate statistical analysis, and functional redundancy of the microbiota. Furthermore, a limitation of the vast majority of previous studies includes the use of 16S-RNA-seq, which does not have enough taxonomic resolution to report results at the species level and does not provide information about microbial functionality. Here, we tackled these limitations by applying a multi-omics approach in three human cohorts and pre-clinical studies.

In concordance with some previous findings (Simpson et al., 2021), we found decreased levels of SCFA-producing bacteria such as species from the *Lachnospiraceae* family (including *Roseburia spp.*) and *Bifidobacterium spp.* (Louis and Flint, 2017). Notably, *Bifidobacterium* strains are among the most efficient GABA producers (Yunes et al., 2016). The current functional metabolomics and metagenomics analyses highlighted several bacterial functions and metabolites involved in proline, histidine, and arginine pathways that converge into glutamate and GABA metabolism linked to depression scores. In line with this, we found that patients with higher PHQ-9 scores had higher levels of *Acidaminococcus spp.*, which use glutamate as the only carbon source and have been shown to grow only in culture media containing arginine, glutamate, or histidine (Dai et al., 2010). Dysregulation of glutamate and GABA neurotransmission and increased circulating levels of glutamate and GABA have been reported in participants with MDD (Duman et al., 2019; Inoshita et al., 2018; Pan et al., 2018). Consistently, we also found that *Acidaminococcus spp.* in the microbiota of recipient mice predicted the expression of gene transcripts in the mPFC that were positively associated with both the donor's depression scores and the recipient mice freezing time, including the GABA (*slc6a12* and *slc6a13*) and proline (*slc6a20a*) transporters. Therefore, the current findings point toward a potential role of the microbiome in depression through glutamate/GABA metabolism, compatible with the glutamate hypothesis of depression (Duman et al., 2019). So far, only two studies have performed functional metagenomics analysis (Stevens et al., 2021; Valles-Colomer et al., 2019). Although not significant, a recent study performing a targeted analysis pointed toward alterations in GABA shunt and glutamate degradation pathways in subjects with depression (Valles-Colomer et al., 2019). Similarly, in a small study (n = 40) the GABA degradation pathway was prominent in the microbiome of individuals with MDD (Stevens et al., 2021).

The most consistent finding was the positive association of circulating proline with the depression scores, and in line with this, dietary proline intake in humans and mouse was positively associated with depression phenotypes. In a recent meta-analysis of peripheral blood metabolites in major depressive disorders, a subgroup analysis revealed that antidepressant-free MDD patients had higher levels of L-proline (Pu et al., 2020). It is worth noting that our analyses were controlled for antidepressant medication. Hyperprolinemia has also been linked to epilepsy, schizophrenia, seizures, and impaired cognitive function in humans (Mitsubuchi et al., 2014; Roussos et al., 2009).

(I) *Gat* pan-glial knockdown in stress-treated males led to a significant decrease in climbing attempts.
(B, F, and J) Stop-for-sweet paradigm. Starved control females, of all genotypes, submitted to mechanical stress treatment stooped less often to eat at a stripe of sucrose when performing negative geotaxis compared with shame-treated females. No significant differences were found between stressed and unstressed females after *Slc6a20* and *Gat* downregulation.
(C, D, G, H, K, and L) Spontaneous locomotor activity, total distance walked during 5 min (C, G, and K), and velocity while in motion during 5 min of tracking activity (D, H, and L).
(C and K) Stress-treated control females of all genotypes walked less and reduced their velocity while in motion, compared with unstressed control flies. No significant differences in total walking distance were observed when (C) *Slc6a20* was neuronally downregulated with RNAi1 or (K) *Gat* was downregulated in glial cells.
(G) No differences in walking distance were observed when *Slc6a20* was pan-neuronally downregulated with RNAi2.
(D, H, and L) No significant differences in velocity while in motion were observed for any knockdown condition.
(M) Experimental timeline followed to generate *Drosophila* wild-type flies under axenic (germ-free) or mono-colonization at the adult stage. After egg sterilization, they were transferred to sterile fly food supplemented with antibiotics. The 1-day-old adults were collected and mono-colonized with *E. cloacae*, *L. plantarum*, or left axenic. Then, 2 days later, the mechanical stress treatment was applied for a period of 5 days; the behavioral tests were performed at day 7 of adulthood.
(N) GAP-climbing assay; *Drosophila* mono-associations at adult stage. A significant decrease in climbing attempts was observed in axenic and mono-colonized *E. cloacae* males, but not in *L. plantarum* mono-colonized males.
(O) Stop-for-sweet paradigm; *Drosophila* mono-associations at adult stage. A significant decrease in percent of stops to eat sucrose line was observed in axenic and mono-colonized *E. cloacae* females, but not in *L. plantarum* mono-colonized males.
A minimum of three biological replicates were tested per each experimental condition. Boxplots represent median and 10 percentile–90 percentile; bar graphs represent mean with SEM. Significance was calculated using non-paramedical Kruskal-Wallis test for multiple comparisons (*$p < 0.05$, **$p < 0.01$, and ***$p < 0.001$).

However, to date, there is no literature describing a direct mechanistic link between proline and depression. Nonetheless, it has been described that animal models with increased concentration of L-proline in the brain present enhanced synaptic activity in hippocampus (Paterlini et al., 2005) and behavioral phenotypes, such as altered performance in cognitive tasks and defects in locomotor activity (Hayward et al., 1993; Kanwar et al., 1975; Paterlini et al., 2005). Moreover, the expression of the proline transporter *SLC6A20*, which mediates cellular proline uptake (Bröer and Gether, 2012; Takanaga et al., 2005), was positively correlated with the donor's PHQ-9 scores and recipient mice freezing time, and we demonstrated that downregulation of *Drosophila slc6a20* in neurons conferred protection against depression-like phenotypes. Additionally, a recent study showed that mice displaying increased expression of *slc620a* presented a reduction in proline and glycine extracellular levels in the brain, decreased NMDAR currents, and repetitive climbing behavior (Bae et al., 2021). Altogether, this indicates that *SLC6A20* may have repercussions in depression phenotypes by modulating proline homeostasis in the brain.

Alternatively, the proline degradative pathway can eventually generate glutamate and GABA. Hence, proline accumulation has been shown to disrupt GABA production and glutamate release and impair synaptic transmission (Crabtree et al., 2016; Wyse and Netto, 2011), whereas inactivation of proline transporter altered glutamatergic synapse and perturbed behaviors in mice (Schulz et al., 2018). In line with previous findings, we found that dietary proline was strongly associated with several pathways involving GABAergic and glutamatergic synapse. We also demonstrated a potential causal role of this amino acid in depression by supplementing mice with proline. Notably, circulating proline levels were consistently associated with nodes of intrinsic brain networks linked to depression. Alterations in the circulating proline levels were also linked to depression cores through the so-called rich club of highly interconnected nodes. The rich club of the brain network plays a critical role in global integration of neural information and is essential for efficient communication across multiple segregated and distant brain regions (Kim and Min, 2020;Escrichs et al., 2021). Therefore, network disruptions within the rich club have a direct impact on various behavioral and cognitive tasks. Connectivity-based neuroimaging studies have identified alterations in rich-club network in several neuropsychiatric disorders (Kim and Min, 2020). Recently, disruptions in the rich-club network organization have also been implicated in MDD (n = 32) (Liu et al., 2021). Here, we extend these findings to mild-moderate depression using a much larger cohort (n = 591).

Dietary proline was also strongly linked to the ECM homeostasis not only in the human intestine but also in the mouse brain. Collagen makes up 80% of ECM, with proline and hydroxyproline accounting for 25% of collagen amino acid content. Therefore, proline is stored in the ECM as collagen, which can serve both as a reservoir and dump for proline (Phang et al., 2010). Of note, components of the ECM such as matrix metalloproteinases, which degrade collagen and release proline, and perineuronal nets have been recently suggested as new key players in the development of psychiatric disorders (Bach et al., 2019). Strikingly, microbiota transfer from humans to mice highlighted a strong upregulation of pathways associated with the ECM and collagen homeostasis as well as GABA- and proline-dependent neurotransmission in the mPFC of mice that received microbiota from human donors with high depression scores. These results further highlight a potential causative role of the microbiome in depression by the disruption of glutamatergic and GABAergic homeostasis through the alteration of proline metabolism. All classical depression treatments directly target the brain with limited effectiveness. Understanding how the microbiome links proline to glutamate and GABA metabolism is thus crucial to design new effective therapies for the treatment of depression. We propose that diets with reduced proline content may have a strong impact in ameliorating depressive symptomatology.

Limitations of study

The current study presents some limitations. A strength of the present study lies in its use of a discovery cohort and a large-scale validation cohort. Although functional results were validated by using a metabolomics approach, one limitation of the study is the lack of shotgun metagenomics data in the validation cohort, which would have provided an additional layer of validation. Second, the longitudinal discovery cohort has a 1-year follow-up. However, a longer term follow-up would be necessary to better understand the strength of our conclusions. Third, the fear conditioning provides an excellent readout of affective learning mechanisms and has a strong anxiety component. The use of other mouse models to test for more specific depressive-like behaviors could strengthen our results. In addition, we only used male mice. Finally, although antibiotics treatment offers a cheaper and accessible alternative to germ-free models, it has the drawbacks of potential off-target drug effects, incomplete eradication of the microbiota, and the lack of standardized antibiotic treatment regimens.

STAR★METHODS

Detailed methods are provided in the online version of this paper and include the following:

- KEY RESOURCES TABLE
- RESOURCE AVAILABILITY
  - Lead contact
  - Materials Availability
  - Data and code availability
- EXPERIMENTAL MODEL AND SUBJECT DETAILS
  - IRONMET cohort (n=116)
  - IRONMET longitudinal cohort (n=70)
  - IMAGEOMICS cohort (n=919)
  - INTESTINE cohort (n=28)
  - ANIMALS (Proline experiment)
  - ANIMALS (FMT experiment)
  - Fly stocks and maintenance
- METHOD DETAILS
  - Clinical and laboratory parameters
  - Body composition
  - Dietary pattern
  - Cognitive assessment
  - MRI acquisition and image pre-processing
  - Intrinsic-ignition framework

- Extraction of fecal genomic DNA and whole-genome shotgun sequencing
- Jejunal stranded RNA sequencing
- Metabolomics analyses
- Proline supplementation mice experiment
- Animals fecal microbiome transplantation (FMT) experiment
- Study of gene expression in the mice prefrontal cortex
- *Drosophila* melanogaster experiments

● QUANTIFICATION AND STATISTICAL ANALYSIS

- Clinical variables
- Metagenomics analyses
- Metabolomics and whole-brain functional dynamics analysis
- RNA-seq analysis

SUPPLEMENTAL INFORMATION

Supplemental information can be found online at https://doi.org/10.1016/j.cmet.2022.04.001.

ACKNOWLEDGMENTS

This work was partially supported by Instituto de Salud Carlos III (Madrid, Spain) through the research grants PI15/01934, PI18/01022, and PI21/01361 to J.M.F.-R. and PI20/01090 (co-funded by the European Regional Development Fund. "A way to make Europe") to J.M.-P.; the Catalan Government (AGAUR, #SGR2017-0734, ICREA Academia Award 2021) to J.M.F.-R.; the Spanish Ministry of Science, Innovation and Universities (PID2019-105969GB-I00); Generalitat Valenciana (Prometeo/2018/133), Spain; and Fondo Europeo de Desarrollo Regional (FEDER) funds to A.M. This work was also supported by the European Commission (FP7, NeuroPain #2013-602891); the Catalan Government (AGAUR, #SGR2017-669, ICREA Academia Award 2020) to R.M.; the Spanish Instituto de Salud Carlos III (RTA, #RD16/0017/0020) to R.M.; Ministry of Science and Innovation and State Research Agency (#PID2020- 120029GB-I00/MICIN/AEI/10.13039/501100011033) to R.M.; the European Regional Development Fund (project no. 01.2.2-LMT-K-718-02-0014) under grant agreement with the Research Council of Lithuania (LMTLT); and the Project ThinkGut (EFA345/19), 65% co-financed by the European Regional Development Fund (ERDF) through the Interreg V-A Spain-France-Andorra program (POCTEFA, 2014–2020). We also acknowledge funding from the Spanish Ministry of Science, Innovation and Universities (RTI2018-099200-B-I00) and the Generalitat of Catalonia (Agency for Management of University and Research Grants [2017SGR696] and Department of Health [SLT002/16/00250]) to R.P. M.A.-R. is funded by Instituto de Salud Carlos III, Río Hortega (CM19/00190). J.M.-P. is funded by a Miguel Servet contract (CP18/00009) from the Instituto de Salud Carlos III. J.S. is funded by a predoctoral PERIS contract (SLT002/16/00250) from the Catalan Government. M.J. is a professor under "Serra Hunter" program (Generalitat de Catalunya). The graphical abstract was created with BioRender.com. We would like to thank Martijn Eidhof for his help in building the stress treatment machine for *Drosophila*.

AUTHOR CONTRIBUTIONS

J.M.-P. researched the data, performed the statistical analysis, and wrote the manuscript. A.C.-N. researched the data and wrote the manuscript. M.A.-R. researched the data. A.C.-N., L.d.v.V.-C., and C.Z. performed the *Drosophila* experiments. A.B., M.M., and R.M. performed or analyzed the experiments in mice. G.B., C.B., A.E., and G.D. researched the MRI data. C.C. performed the neuropsychological examination. J.M.M.-N. performed the RNA sequencing of jejunal samples. V.P.-B. and A.M. contributed with the determination and analysis of the microbiota. J.P., J.G.-O., R.R., S.P., R.B., J.C.V., J. Serena, J.G., L.R.-T., and W.R. contributed to the discussion and reviewed the manuscript. M.J., R.P., J. Sol., and M.P.-O. performed the metabolomics analyses. J.M.-P. and J.M.F.-R. carried out the conception and coordination of the study, performed the statistical analysis, and wrote the manuscript. All authors participated in the final approval of the version to be published. J.M.F.-R. is the guarantor of this work and thus had full access to all the data in the study and takes responsibility for the integrity of the data.

DECLARATION OF INTERESTS

The authors declare no competing interests.

INCLUSION AND DIVERSITY

For studies involving human subjects, whether recruited (e.g. clinical analyses) or enrolled spontaneously (e.g. online surveys), we worked to ensure gender balance in the recruitment of human subjects. We worked to ensure ethnic or other types of diversity in the recruitment of human subjects. We worked to ensure that the study questionnaires were prepared in an inclusive way.

Received: May 6, 2021
Revised: January 31, 2022
Accepted: April 4, 2022
Published: May 3, 2022

REFERENCES

Arnoriaga-Rodríguez, M., Mayneris-Perxachs, J., Burokas, A., Contreras-Rodríguez, O., Blasco, G., Coll, C., Biarnés, C., Miranda-Olivos, R., Latorre, J., Moreno-Navarrete, J.M., et al. (2020). Obesity impairs short-term and working memory through gut microbial metabolism of aromatic amino acids. Cell Metab. *32*, 548–560.e7.

Arnoriaga-Rodríguez, M., Mayneris-Perxachs, J., Contreras-Rodríguez, O., Burokas, A., Ortega-Sanchez, J.-A., Blasco, G., Coll, C., Biarnés, C., Castells-Nobau, A., Puig, J., et al. (2021). Obesity-associated deficits in inhibitory control are phenocopied to mice through gut microbiota changes in one-carbon and aromatic amino acids metabolic pathways. Gut *70*, 2283–2296.

Asmar, R. El, Panigrahi, P., Bamford, P., Berti, I., Not, T., Coppa, G.V., Catassi, C., and Fasano, A. (2002). Host-dependent zonulin secretion causes the impairment of the small intestine barrier function after bacterial exposure. Gastroenterology *123*, 1607–1615.

Bach, D.R., Brown, S.A., Kleim, B., and Tyagarajan, S.K. (2019). Extracellular matrix: a new player in memory maintenance and psychiatric disorders. Swiss Med. Wkly. *149*, w20060.

Bae, M., Roh, J.D., Kim, Y., Kim, S.S., Han, H.M., Yang, E., Kang, H., Lee, S., Kim, J.Y., Kang, R., et al. (2021). SLC6A20 transporter: a novel regulator of brain glycine homeostasis and NMDAR function. EMBO Mol. Med. *13*, e12632.

Branson, K., Robie, A.A., Bender, J., Perona, P., and Dickinson, M.H. (2009). High-throughput ethomics in large groups of *Drosophila*. Nat. Methods *6*, 451–457.

Broderick, N.A., and Lemaitre, B. (2012). Gut-associated microbes of *Drosophila melanogaster*. Gut Microbes *3*, 307–321.

Bröer, S., and Gether, U. (2012). The solute carrier 6 family of transporters. Br. J. Pharmacol. *167*, 256–278.

Carvajal-Rodríguez, A., de Uña-Alvarez, J., and Rolán-Alvarez, E. (2009). A new multitest correction (SGoF) that increases its statistical power when increasing the number of tests. BMC Bioinformatics *10*, 209.

Castells-Nobau, A., Eidhof, I., Fenckova, M., Brenman-Suttner, D.B., Scheffer-De Gooyert, J.M., Christine, S., Schellevis, R.L., Van Der Laan, K., Quentin, C., Van Ninhuijs, L., et al. (2019). Conserved regulation of neurodevelopmental processes and behavior by FoxP in *Drosophila*. PLoS One *14*, e0211652.

Crabtree, G.W., Park, A.J., Gordon, J.A., and Gogos, J.A. (2016). Cytosolic accumulation of L-proline disrupts GABA-Ergic transmission through GAD blockade. Cell Rep. *17*, 570–582.

Cryan, J.F., O'Riordan, K.J., Cowan, C.S.M., Sandhu, K.V., Bastiaanssen, T.F.S., Boehme, M., Codagnone, M.G., Cussotto, S., Fulling, C.,

Golubeva, A.V., et al. (2019). The microbiota-gut-brain axis. Physiol. Rev. *99*, 1877–2013.

Cui, Y., Miao, K., Niyaphorn, S., and Qu, X. (2020). Production of gamma-aminobutyric acid from lactic acid bacteria: a systematic review. Int. J. Mol. Sci. *21*, 995.

Dai, Z.L., Zhang, J., Wu, G., and Zhu, W.Y. (2010). Utilization of amino acids by bacteria from the pig small intestine. Amino Acids *39*, 1201–1215.

Deco, G., and Kringelbach, M.L. (2017). Hierarchy of information processing in the brain: a novel "intrinsic ignition" framework. Neuron *94*, 961–968.

Degenhardt, F., Seifert, S., and Szymczak, S. (2019). Evaluation of variable selection methods for random forests and omics data sets. Brief. Bioinform. *20*, 492–503.

Dobin, A., Davis, C.A., Schlesinger, F., Drenkow, J., Zaleski, C., Jha, S., Batut, P., Chaisson, M., and Gingeras, T.R. (2013). STAR: ultrafast universal RNA-seq aligner. Bioinformatics *29*, 15–21.

Duman, R.S., Sanacora, G., and Krystal, J.H. (2019). Altered connectivity in depression: GABA and glutamate neurotransmitter deficits and reversal by novel treatments. Neuron *102*, 75–90.

Durbin, R., Eddy, S.R., Krogh, A., and Mitchison, G. (1998). Biological Sequence Analysis: Probabilistic Models of Proteins and Nucleic Acids (Cambridge).

Escrichs, A., Biarnes, C., Garre-Olmo, J., Fernández-Real, J.M., Ramos, R., Pamplona, R., Brugada, R., Serena, J., Ramió-Torrentà, L., Coll-De-Tuero, G., et al. (2021). Whole-brain dynamics in aging: disruptions in functional connectivity and the role of the rich club. Cereb. Cortex *31*, 2466–2481.

Farley, S., Apazoglou, K., Witkin, J.M., Giros, B., and Tzavara, E.T. (2010). Antidepressant-like effects of an AMPA receptor potentiator under a chronic mild stress paradigm. Int. J. Neuropsychopharmacol. *13*, 1207–1218.

Fasano, A. (2012). Zonulin, regulation of tight junctions, and autoimmune diseases. Ann. N. Y. Acad. Sci. *1258*, 25–33.

Fernandes, A.D., Reid, J.N.S., Macklaim, J.M., McMurrough, T.A., Edgell, D.R., and Gloor, G.B. (2014). Unifying the analysis of high-throughput sequencing datasets: characterizing RNA-seq, 16S rRNA gene sequencing and selective growth experiments by compositional data analysis. Microbiome *2*, 15.

Gloor, G.B., Macklaim, J.M., Pawlowsky-Glahn, V., and Egozcue, J.J. (2017). Microbiome datasets are compositional: and this is not optional. Front. Microbiol. *8*, 2224.

Hansen, R., Gaynes, B., Thieda, P., Gartlehner, G., Deveaugh-Geiss, A., Krebs, E., and Lohr, K. (2008). Meta-analysis of major depressive disorder relapse and recurrence with second-generation antidepressants. Psychiatr. Serv. *59*, 1121–1130.

Hayward, D.C., Delaney, S.J., Campbell, H.D., Ghysen, A., Benzer, S., Kasprzak, A.B., Cotsell, J.N., Young, I.G., and Miklos, G.L.G. (1993). The sluggish-A gene of *Drosophila melanogaster* is expressed in the nervous system and encodes proline oxidase, a mitochondrial enzyme involved in glutamate biosynthesis. Proc. Natl. Acad. Sci. USA *90*, 2979–2983.

Hyatt, D., Chen, G.L., LoCascio, P.F., Land, M.L., Larimer, F.W., and Hauser, L.J. (2010). Prodigal: prokaryotic gene recognition and translation initiation site identification. BMC Bioinformatics *11*, 119.

Imma Palma, D., Farran, A., and Pilar Cervera, S. (2008). Tablas de composición de alimentos por medidas caseras de consumo habitual en España. Act. Diet. *12*, 85.

Inoshita, M., Umehara, H., Watanabe, S.Y., Nakataki, M., Kinoshita, M., Tomioka, Y., Tajima, A., Numata, S., and Ohmori, T. (2018). Elevated peripheral blood glutamate levels in major depressive disorder. Neuropsychiatr. Dis. Treat. *14*, 945–953.

Jacobs, J.P., Lin, L., Goudarzi, M., Ruegger, P., McGovern, D.P., Fornace, A.J., Borneman, J., Xia, L., and Braun, J. (2017). Microbial, metabolomic, and immunologic dynamics in a relapsing genetic mouse model of colitis induced by T-synthase deficiency. Gut Microbes *8*, 1–16.

James, S.L., Abate, D., Abate, K.H., Abay, S.M., Abbafati, C., Abbasi, N., Abbastabar, H., Abd-Allah, F., Abdela, J., and Abdelalim, A. (2018). Global, regional, and national incidence, prevalence, and years lived with disability for 354 diseases and injuries for 195 countries and territories, 1990–2017: a systematic analysis for the Global Burden of Disease Study 2017. Lancet *392*, 1789–1858.

Kamburov, A., Stelzl, U., Lehrach, H., and Herwig, R. (2013). The ConsensusPathDB interaction database: 2013 Update. Nucleic Acids Res. *41*, D793–D800.

Kanehisa, M., and Goto, S. (2000). KEGG: Kyoto encyclopedia of genes and genomes. Nucleic Acids Res. *28*, 27–30.

Kanwar, Y.S., Krakower, C.A., Manaligod, J.R., Justice, P., and Wong, P.W. (1975). Biochemical, morphological and hybrid studies in hyperprolinemic mice. Biomedicine *22*, 209–216.

Kim, D.J., and Min, B.K. (2020). Rich-club in the brain's macrostructure: insights from graph theoretical analysis. Comput. Struct. Biotechnol. J. *18*, 1761–1773.

Kim, J., and Wessling-Resnick, M. (2014). Iron and mechanisms of emotional behavior. J. Nutr. Biochem. *25*, 1101–1107.

Kitajima, H., Shiomoto, H., Osada, K., and Yokogoshi, H. (2003). Co-administration of proline and inorganic iron enhance the improvement of behavioral and hematological function of iron-deficient anemic rats. J. Nutr. Sci. Vitaminol. *49*, 7–12.

Koyle, M.L., Veloz, M., Judd, A.M., Wong, A.C.N., Newell, P.D., Douglas, A.E., and Chaston, J.M. (2016). Rearing the fruit fly *Drosophila melanogaster* under axenic and gnotobiotic conditions. J. Vis. Exp. *113*, 54219.

Kroenke, K., Spitzer, R.L., and Williams, J.B.W. (2001). The PHQ-9: validity of a brief depression severity measure. J. Gen. Intern. Med. *16*, 606–613.

Kursa, M.B., and Rudnicki, W.R. (2010). Feature selection with the boruta package. J. Stat. Softw. *36*, 1–13.

Langgartner, D., Marks, J., Nguyen, T.C., and Reber, S.O. (2020). Changes in adrenal functioning induced by chronic psychosocial stress in male mice: a time course study. Psychoneuroendocrinology *122*, 104880.

Langmead, B., and Salzberg, S.L. (2012). Fast gapped-read alignment with Bowtie 2. Nat. Methods *9*, 357–359.

Li, B., and Dewey, C.N. (2011). RSEM: accurate transcript quantification from RNA-seq data with or without a reference genome. BMC Bioinformatics *12*, 323.

Li, D., Liu, C.M., Luo, R., Sadakane, K., and Lam, T.W. (2015). MEGAHIT: an ultra-fast single-node solution for large and complex metagenomics assembly via succinct de Bruijn graph. Bioinformatics *31*, 1674–1676.

Liang, S., Wu, X., Hu, X., Wang, T., and Jin, F. (2018). Recognizing depression from the microbiota-gut-brain axis. Int. J. Mol. Sci. *19*, 1592.

Liao, Y., Smyth, G.K., and Shi, W. (2014). FeatureCounts: an efficient general purpose program for assigning sequence reads to genomic features. Bioinformatics *30*, 923–930.

Liu, X., He, C., Fan, D., Zhu, Y., Zang, F., Wang, Q., Zhang, H., Zhang, Z., Zhang, H., and Xie, C. (2021). Disrupted rich-club network organization and individualized identification of patients with major depressive disorder. Prog. Neuropsychopharmacol. Biol. Psychiatry *108*, 110074.

Louis, P., and Flint, H.J. (2017). Formation of propionate and butyrate by the human colonic microbiota. Environ. Microbiol. *19*, 29–41.

Love, M.I., Huber, W., and Anders, S. (2014). Moderated estimation of fold change and dispersion for RNA-seq data with DESeq2. Genome Biol. *15*, 550–550.

Maes, M., Kubera, M., Leunis, J.C., and Berk, M. (2012). Increased IgA and IgM responses against gut commensals in chronic depression: further evidence for increased bacterial translocation or leaky gut. J. Affect. Disord. *141*, 55–62.

Magoč, T., and Salzberg, S.L. (2011). FLASH: fast length adjustment of short reads to improve genome assemblies. Bioinformatics *27*, 2957–2963.

Mato, S., Aso, E., Castro, E., Martín, M., Valverde, O., Maldonado, R., and Pazos, Á. (2007). CB1 knockout mice display impaired functionality of 5-HT 1A and 5-HT2A/C receptors. J. Neurochem. *103*, 2111–2120.

Mayneris-Perxachs, J., and Fernández-Real, J.M. (2020). Exploration of the microbiota and metabolites within body fluids could pinpoint novel disease mechanisms. FEBS J. *287*, 856–865.

Menzel, P., Ng, K.L., and Krogh, A. (2016). Fast and sensitive taxonomic classification for metagenomics with Kaiju. Nat. Commun. *7*, 11257.

Merico, D., Isserlin, R., Stueker, O., Emili, A., and Bader, G.D. (2010). Enrichment map: a network-based method for gene-set enrichment visualization and interpretation. PLoS One *5*, e13984.

Merkling, S.H., and Van Rij, R.P. (2015). Analysis of resistance and tolerance to virus infection in *Drosophila*. Nat. Protoc. *10*, 1084–1097.

Mitsubuchi, H., Nakamura, K., Matsumoto, S., and Endo, F. (2014). Biochemical and clinical features of hereditary hyperprolinemia. Pediatr. Int. *56*, 492–496.

Moriguchi, S., Takamiya, A., Noda, Y., Horita, N., Wada, M., Tsugawa, S., Plitman, E., Sano, Y., Tarumi, R., ElSalhy, M., et al. (2019). Glutamatergic neurometabolite levels in major depressive disorder: a systematic review and meta-analysis of proton magnetic resonance spectroscopy studies. Mol. Psychiatry *24*, 952–964.

Pan, J.X., Xia, J.J., Deng, F.L., Liang, W.W., Wu, J., Yin, B.M., Dong, M.X., Chen, J.J., Ye, F., Wang, H.Y., et al. (2018). Diagnosis of major depressive disorder based on changes in multiple plasma neurotransmitters: a targeted metabolomics study. Transl. Psychiatry *8*, 130.

Paterlini, M., Zakharenko, S.S., Lai, W.S., Qin, J., Zhang, H., Mukai, J., Westphal, K.G.C., Olivier, B., Sulzer, D., Pavlidis, P., et al. (2005). Transcriptional and behavioral interaction between 22q11.2 orthologs modulates schizophrenia-related phenotypes in mice. Nat. Neurosci. *8*, 1586–1594.

Paxinos, G., and Franklin, K.B.J. (1997). The Mouse Brain in Stereotaxic Coordinates (Academic Press).

Phang, J.M., Liu, W., and Zabirnyk, O. (2010). Proline metabolism and microenvironmental stress. Annu. Rev. Nutr. *30*, 441–463.

Pick, S., and Strauss, R. (2005). Goal-driven behavioral adaptations in gap-climbing *Drosophila*. Curr. Biol. *15*, 1473–1478.

Pu, J., Liu, Y., Zhang, H., Tian, L., Gui, S., Yu, Y., Chen, X., Chen, Y., Yang, L., Ran, Y., et al. (2020). An integrated meta-analysis of peripheral blood metabolites and biological functions in major depressive disorder. Mol. Psychiatry *26*, 4265–4276.

Puig, J., Biarnes, C., Pedraza, S., Vilanova, J.C., Pamplona, R., Fernández-Real, J.M., Brugada, R., Ramos, R., Coll-de-Tuero, G., Calvo-Perxas, L., et al. (2020). The aging imageomics study: rationale, design and baseline characteristics of the study population. Mech. Ageing Dev. *189*, 111257.

R Development Core Team. (2013). R: A language and environment for statistical computing (R Foundation for Statistical Computing).

Ries, A.S., Hermanns, T., Poeck, B., and Strauss, R. (2017). Serotonin modulates a depression-like state in *Drosophila* responsive to lithium treatment. Nat. Commun. *8*, 15738.

Ritchie, M.E., Phipson, B., Wu, D., Hu, Y., Law, C.W., Shi, W., and Smyth, G.K. (2015). Limma powers differential expression analyses for RNA-sequencing and microarray studies. Nucleic Acids Res. *43*, e47.

Robinson, M.D., McCarthy, D.J., and Smyth, G.K. (2010). edgeR: a Bioconductor package for differential expression analysis of digital gene expression data. Bioinformatics *26*, 139–140.

Roussos, P., Giakoumaki, S.G., and Bitsios, P. (2009). A risk PRODH haplotype affects sensorimotor gating, memory, schizotypy, and anxiety in healthy male subjects. Biol. Psychiatry *65*, 1063–1070.

Saravia, R., Ten-Blanco, M., Julià-Hernández, M., Gagliano, H., Andero, R., Armario, A., Maldonado, R., and Berrendero, F. (2019). Concomitant THC and stress adolescent exposure induces impaired fear extinction and related neurobiological changes in adulthood. Neuropharmacology *144*, 345–357.

Schmieder, R., and Edwards, R. (2011). Quality control and preprocessing of metagenomic datasets. Bioinformatics *27*, 863–864.

Schulz, D., Morschel, J., Schuster, S., Eulenburg, V., and Gomeza, J. (2018). Inactivation of the mouse L-proline transporter PROT alters glutamatergic synapse biochemistry and perturbs behaviors required to respond to environmental changes. Front. Mol. Neurosci. *11*, 279.

Simpson, C.A., Diaz-Arteche, C., Eliby, D., Schwartz, O.S., Simmons, J.G., and Cowan, C.S.M. (2021). The gut microbiota in anxiety and depression—a systematic review. Clin. Psychol. Rev. *83*, 101943.

Sonnenburg, J.L., and Bäckhed, F. (2016). Diet-microbiota interactions as moderators of human metabolism. Nature *535*, 56–64.

Spitzer, R.L., Kroenke, K., and Williams, J.B.W. (1999). Validation and utility of a self-report version of PRIME-MD: the PHQ primary care study. Primary care evaluation of mental disorders. Patient health questionnaire. J. Am. Med. Assoc. *282*, 1737–1744.

Stevens, B.R., Goel, R., Seungbum, K., Richards, E.M., Holbert, R.C., Pepine, C.J., and Raizada, M.K. (2018). Increased human intestinal barrier permeability plasma biomarkers zonulin and FABP2 correlated with plasma LPS and altered gut microbiome in anxiety or depression. Gut *67*, 1555–1557.

Stevens, B.R., Roesch, L., Thiago, P., Russell, J.T., Pepine, C.J., Holbert, R.C., Raizada, M.K., and Triplett, E.W. (2021). Depression phenotype identified by using single nucleotide exact amplicon sequence variants of the human gut microbiome. Mol. Psychiatry *26*, 4277–4287.

Strandwitz, P. (2018). Neurotransmitter modulation by the gut microbiota. Brain Res. *1693*, 128–133.

Surget, A., Tanti, A., Leonardo, E.D., Laugeray, A., Rainer, Q., Touma, C., Palme, R., Griebel, G., Ibarguen-Vargas, Y., Hen, R., and Belzung, C. (2011). Antidepressants recruit new neurons to improve stress response regulation. Mol. Psychiatry *16*, 1177–1188.

Szklarczyk, D., Gable, A.L., Lyon, D., Junge, A., Wyder, S., Huerta-Cepas, J., Simonovic, M., Doncheva, N.T., Morris, J.H., Bork, P., et al. (2019). STRING v11: protein-protein association networks with increased coverage, supporting functional discovery in genome-wide experimental datasets. Nucleic Acids Res. *47*, D607–D613.

Takanaga, H., Mackenzie, B., Suzuki, Y., and Hediger, M.A. (2005). Identification of mammalian proline transporter SIT1 (SLC6A20) with characteristics of classical system imino. J. Biol. Chem. *280*, 8974–8984.

Valles-Colomer, M., Falony, G., Darzi, Y., Tigchelaar, E.F., Wang, J., Tito, R.Y., Schiweck, C., Kurilshikov, A., Joossens, M., Wijmenga, C., et al. (2019). The neuroactive potential of the human gut microbiota in quality of life and depression. Nat. Microbiol. *4*, 623–632.

Vioque, J., Navarrete-Muñoz, E.-M., Gimenez-Monzó, D., García-de-la-Hera, M., Granado, F., Young, I.S., Ramón, R., Ballester, F., Murcia, M., Rebagliato, M., et al. (2013). Reproducibility and validity of a food frequency questionnaire among pregnant women in a Mediterranean area. Nutr. J. *12*, 26.

Wang, L., Hermens, D.F., Hickie, I.B., and Lagopoulos, J. (2012). A systematic review of resting-state functional-MRI studies in major depression. J. Affect. Disord. *142*, 6–12.

Wikoff, W.R., Pendyala, G., Siuzdak, G., and Fox, H.S. (2008). Metabolomic analysis of the cerebrospinal fluid reveals changes in phospholipase expression in the CNS of SIV-infected macaques. J. Clin. Invest. *118*, 2661–2669.

Willett, W.C., Sampson, L., Stampfer, M.J., Rosner, B., Bain, C., Witschi, J., Hennekens, C.H., and Speizer, F.E. (1985). Reproducibility and validity of a semiquantitative food frequency questionnaire. Am. J. Epidemiol. *122*, 51–65.

World Health Organization (2020). Depression. https://www.who.int/news-room/fact-sheets/detail/depression

World Health Organization. (2006). Safety evaluation of certain contaminants in food. Prepared by the sixty-fourth meeting of the Joint FAO/WHO Expert Committee on Food Additives (JECFA). FAO Food Nutr. Pap. *82*, 435–480.

Wu, G.D., Chen, J., Hoffmann, C., Bittinger, K., Chen, Y.Y., Keilbaugh, S.A., Bewtra, M., Knights, D., Walters, W.A., Knight, R., et al. (2011). Linking long-term dietary patterns with gut microbial enterotypes. Science *334*, 105–108.

Wyse, A.T.S., and Netto, C.A. (2011). Behavioral and neurochemical effects of proline. Metab. Brain Dis. *26*, 159–172.

Yunes, R.A., Poluektova, E.U., Dyachkova, M.S., Klimina, K.M., Kovtun, A.S., Averina, O.V., Orlova, V.S., and Danilenko, V.N. (2016). GABA production and

structure of gadB/gadC genes in Lactobacillus and Bifidobacterium strains from human microbiota. Anaerobe *42*, 197–204.

Zecca, L., Youdim, M.B.H., Riederer, P., Connor, J.R., and Crichton, R.R. (2004). Iron, brain ageing and neurodegenerative disorders. Nat. Rev. Neurosci. *5*, 863–873.

Zhou, X., Teng, T., Zhang, Y., Del Giovane, C., Furukawa, T.A., Weisz, J.R., Li, X., Cuijpers, P., Coghill, D., Xiang, Y., et al. (2020). Comparative efficacy and acceptability of antidepressants, psychotherapies, and their combination for acute treatment of children and adolescents with depressive disorder: a systematic review and network meta-analysis. Lancet Psychiatry *7*, 581–601.

STAR★METHODS

KEY RESOURCES TABLE

REAGENT or RESOURCE	SOURCE	IDENTIFIER
Biological samples		
Human body fluids (feces, plasma)	This paper	N/A
Mice feces	This paper	N/A
Mice prefrontal cortex	This paper	N/A
Chemicals, peptides, and recombinant proteins		
3-(Trimethylsilyl)propionic-2,2,3,3-d4 acid sodium salt (TSP)	Sigma-Aldrich	Cat# 269913
Disodium hydrogen phosphate	Sigma-Aldrich	Cat#1.06586
Sodium dihydrogen phosphate	Sigma-Aldrich	Cat#1.06370
Deuterated water 99.8%	Thermo Fisher Scientific	Cat#10255880
Methanol LC-MS	Scharlau	Cat#ME03262500
Lysing Matrix E	MP biomedicals	Cat#SKU116914050-CF
Acetic acid LC-MS	Scharlau	Cat#AC03470050
L-proline	Sigma-Aldrich	Cat#P0380
RNAlater Stabilization Solution	Thermo Fisher Scientific	Cat#AM7020
Critical commercial assays		
QIAamp DNA mini stool kit	Qiagen	Cat#51504
Nextera DNA Flex Library Preparation kit	Illumina	Cat#20018705
ALLPrep DNA/RNA/miRNA Universal kit	Qiagen	Cat#80224
TrueSeq stranded mRNA library preparation kit	Illumina	Cat#20020594
Truseq RNA Single Indexes	Illumina	Cat#20020492
Truseq RNA Single Indexes	Illumina	Cat#20020493
RNA 6000 Nano chip	Agilent	Cat#5067-1511
DNA 1000 chip	Agilent	Cat#5067-1504
KAPA Library Quantification Kit	Roche	Cat#07960204001
RNeasy Mini-Kit	Qiagen	Cat#74104
RNA kit (15NT)	Agilent	Cat#DNF-471-0500
Truseq stranded Total RNA Library Prep	Illumina	Cat#20020596
Illumina Ribo-Zero Plus rRNA Depletion kit	Illumina	Cat#20040526
LBP mouse ELISA kit	HyCult Biotech	Cat#HK205-02
Human LBP ELISA kit	HyCult Biotech	Cat#K5601
Deposited data		
Metagenome Sequencing Data of Fecal Samples from Human subjects and Mice	European Nucleotide Archive (ENA)	Project number: PRJEB39631; Human samples accession numbers: ERS4859818-ERS4859933; Mice samples accession numbers: ERS4859934-ERS4859966
Experimental models: Organisms/strains		
Mouse CD-1	Charles River	N/A
Drosophila Melanogaster	BestGene	N/A
Lactobacillus Plantarum DSM 2601	Leibniz Institute DSMZ	N/A
Enterobacter cloacae DSM 6234	Leibniz Institute DSMZ	N/A
Software and algorithms		
SPSS software (version 19)	IBM	https://www.ibm.com/analytics/spss-statistics-software
Prism (version 9.3.1)	Graphpad	https://www.graphpad.com/

(*Continued on next page*)

Continued

REAGENT or RESOURCE	SOURCE	IDENTIFIER
Rstudio (version 1.3.959)	Rstudio Team	https://rstudio.com/
R (version 3.6)	R	https://www.r-project.org/
MassHunter Data Analysis software	Agilent Technologies	Cat#RRID: SCR_015040
Prinseq-lite-0.20.4	(Schmieder and Edwards, 2011)	http://prinseq.sourceforge.net/
FLASH 1.2.11	(Magoč and Salzberg, 2011)	https://ccb.jhu.edu/software/FLASH/
Bowtie2-2.3.4.3	(Langmead and Salzberg, 2012)	http://bowtie-bio.sourceforge.net/bowtie2/index.shtml
MEGAHIT v1.1.2	(Li et al., 2015)	https://github.com/voutcn/megahit
Prodigal v2.6.342	(Hyatt et al., 2010)	https://github.com/hyattpd/Prodigal
HMMER	(Durbin et al., 1998)	http://hmmer.org/
Kaiju v1.6.2	(Menzel et al., 2016)	https://github.com/bioinformatics-centre/kaiju
STAR software (version 2.5.3a)	(Dobin et al., 2013)	https://github.com/alexdobin/STAR
Subread (version 1.5.1)	(Liao et al., 2014)	http://subread.sourceforge.net/
RSEM (version 1.3.0)	(Li and Dewey, 2011)	https://deweylab.github.io/RSEM/
Limma (version 3.30.13)	(Ritchie et al., 2015)	https://bioconductor.org/packages/release/bioc/html/limma.html
edgeR (version 3.26.8)	(Robinson et al., 2010)	https://bioconductor.org/packages/release/bioc/html/edgeR.html
DESeq2 (version 1.26.0)	(Love et al., 2014)	https://bioconductor.org/packages/release/bioc/html/DESeq2.html
ALDEx2 (version 1.18.0)	(Fernandes et al., 2014)	https://www.bioconductor.org/packages/release/bioc/html/ALDEx2.html
SGoF (version 2.3.2)	(Carvajal-Rodríguez et al., 2009)	https://cran.r-project.org/web/packages/sgof/index.html
STRING (version 11.0b)	(Szklarczyk et al., 2019).	https://string-db.org/
Consensus Pathway Data Base (CPDB)	(Kamburov et al., 2013)	http://cpdb.molgen.mpg.de/
Boruta (version 6.0.0)	(Kursa and Rudnicki, 2010)	https://cran.r-project.org/web/packages/Boruta/
Ctrax (version 0.5.18)	(Branson et al., 2009)	http://ctrax.sourceforge.net/
Other		
Avance III 600 spectrometer	Bruker	N/A
5Mmm PABBO gradient probe	Bruker	N/A
Dual energy X-ray absorptiometry	GE Healthcare	N/A
Cobas 8000 c702 analyzer	Roche Diagnostics	N/A
ADAM A1c HA-8180V	ARKRAY	N/A
Shuttle chamber LE918	Panlab	N/A
Bioanalyzer 2100	Agilent	N/A
ABI 7900HT qPCR	Applied Biosystems	N/A
Qubit 3.0 fluorometer	Thermo Fisher Scientific	N/A
HiSeq 2500	Illumina	N/A
NextSeq 500	Illumina	N/A
NovaSeq 6000	Illumina	N/A
LightCycler 480 II	Roche	N/A
5300 Fragment Analyzer System	Agilent	N/A
Micro-plate shaker LD 450 Digital	Labinco	N/A
Standard diet, RM1 (P), Special Diets Services, Essex, UK. Irradiated Vacuum packed	Dietex International	#801151

RESOURCE AVAILABILITY

Lead contact

Further information and requests for resources and reagents should be directed to and will be fulfilled by the lead contact, José Manuel Fernández-Real (jmfreal@idibgi.org).

Materials Availability

This study did not generate new unique reagents.

Data and code availability

- The raw metagenomic sequence data derived from human samples in the IRONMET cohort and mouse samples have been deposited in the European Nucleotide Archive (ENA) an accession numbers are listed in the key resources table.
- This paper does not report original code.
- Any additional information required to reanalyze the data reported in this paper is available from the lead contact upon request.

EXPERIMENTAL MODEL AND SUBJECT DETAILS

IRONMET cohort (n=116)

This is a cross-sectional case-control study setting at the Endocrinology Department of Dr. Josep Trueta University Hospital. The recruitment of subjects started in January 2016 and finished in October 2017. Consecutive middle-aged subjects, 27.2–66.6 years, were included. Patients with obesity (body mass index (BMI) $\geq$30 kg/m^2) and age-matched and sex-matched subjects without obesity (BMI 18.5–<30 kg/m^2) were eligible. Exclusion criteria were type 2 diabetes mellitus, chronic inflammatory systemic diseases, acute or chronic infections in the previous month; use of antibiotic, antifungal, antiviral or treatment with proton pump inhibitors; severe disorders of eating behavior or major psychiatric antecedents; neurological diseases, history of trauma or injured brain, language disorders and excessive alcohol intake ($\geq$40 g OH/day in women or 80 g OH/day in men). The Institutional review board - Ethics Committee and the Committee for Clinical Research (CEIC) of Dr. Josep Trueta University Hospital (Girona, Spain) approved the study protocol and informed written consent was obtained from all participants.

IRONMET longitudinal cohort (n=70)

After 1-year of follow-up individuals were re-evaluated and cognitive function, brain structure and fecal and plasma samples were collected.

IMAGEOMICS cohort (n=919)

The Ageing Imageomics Study is an observational study including participants from two independent cohort studies (MESGI50 and MARK). Detailed description of the cohorts can be found elsewhere (Puig et al., 2020). Briefly, the MESGI50 cohort included a population aged $\geq$50 years, while the MARK cohort included a random sample of patients aged 35–74 years with intermediate cardiovascular risk. Eligibility criteria included age $\geq$50 years, dwelling in the community, no history of infection during the last 15 days, no contraindications for MRI and consent to be informed of potential incidental findings.

INTESTINE cohort (n=28)

This is a pilot project that included morbidly obese (BMI >35 kg/m^2) subjects recruited at the Endocrinology Department of Dr. Josep Trueta University Hospital. All subjects were of Caucasian origin and reported a body weight stable for at least three months before the study. Subjects were studied in the post-absorptive state. The following exclusion criteria were considered: i) no systemic disease other than obesity; ii) free of any infections in the previous month before the study; iii) no liver diseases (specifically tumor disease and infections) and thyroid dysfunction, which will be specifically excluded by biochemical work-up. This protocol was revised, validated and approved by the Ethics committee of the Hospital Dr Josep Trueta. The purpose of the study was explained to participants and they signed written informed consent before being enrolled in the study.

The characteristics of the human cohorts can be found in Table S1

ANIMALS (Proline experiment)

Male CD-1 mice (8 weeks old at the beginning of the experiment) were used. Animals were housed in reverse light-dark cycle (lights on from 20:00 to 8:00), standard temperature (21° +/- 1° C) and with food and water available ad libitum. Mice exposed to the Unpredictable Chronic Mild Stress (UCMS) procedure were singled housed in one room. Control mice, not exposed to UCMS, were housed 2-4 per cage in a different room. Animals were divided into the following experimental groups. Ten control mice were exposed to standard diet and water for the entire experimental procedure. Similarly, mice exposed to the UCMS protocol were divided in the following 2 groups of 10 mice each: i) standard diet and water, ii) standard diet and L-proline (Sigma-Aldrich P0380) diluted in the drinking water (36 g/l). L-proline was freshly prepared and replaced every 3-4 days. All animal procedures were performed in accordance with the guidelines of the European Communities Council Directive 2010/63/EU regulating animal research and were approved by the local ethical committee (Comitè Ètic d'Experimentació Animal-Parc de Recerca Biomèdica de Barcelona, CEEA-PRBB).

ANIMALS (FMT experiment)

Male CD-1 mice (Male JAX CD-1wild-type (WT) mice, purchased from Charles River (Lyon, France)), weighing 23–26 g at the beginning of the experiment were used. Upon arrival to the animal facilities, animals were let to adapt during 5 days to housing conditions (12 hours reversed light/dark cycle, 08:00 AM lights off). Mice were housed individually in controlled laboratory conditions with

temperature maintained at 21±1 °C and humidity at 55 ± 10%. All animals were fed a standard chow diet RM1 (Standard diet, #801151 RM1 (P), Special Diets Services, Essex, UK. Irradiated Vacuum packed, Dietex International). Food and water were available *ad libitum* during all the experiment. The health status of each mouse included in the experimental schedule was checked every day before the experimental sessions and recorded in the experimenter protocol notebook. Health status checks included body weight, physical aspect, behavior, and clinical signs. No abnormalities were recorded in the animals included in this study. All animal procedures were performed in accordance with the guidelines of the European Communities Council Directive 2010/63/EU regulating animal research and were approved by the local ethical committee (Comitè Ètic d'Experimentació Animal-Parc de Recerca Biomèdica de Barcelona, CEEA-PRBB).

Fly stocks and maintenance

Flies were raised on standard medium (cornmeal, sugar, yeast). The following genetic strains were obtained from the Bloomington stocks center (Indiana University): *w;;elav-GAL4* (8760) and *Repo-GAL4* (7415). Conditional RNAi lines targeting *CG43066 the Drosophila* orthologue of *Slc6a20* (stocks 101768 and 37183, referred as *Slc6a20-RNAi1* and *Slc6a20-RNAi1*, respectively), *Gat-RNAi* (106638), genetic background controls (60100 and 60000 referred as Control1 and Control2, respectively) and *UAS-Dcr2* (60009) were obtained from the Vienna *Drosophila* RNAi Centre (VDRC, Vienna, Austria). The *Drosophila* wild-type strain used in this study was originally obtained from Bestgene. The final stock was created by exchanging the w^- allele of the strain that the company regularly uses to inject P-element-based transgenes by a w^+ allele (Castells-Nobau et al., 2019).

Crosses using the *UAS-Dcr2; elav-GAL4* driver line, were raised at 28 degrees. Crosses with *Repo-GAL4* driver, mono-colonized or axenic flies, all behavioral experiments and depression induction by mechanical-stress were performed at 25 degrees. All flies were maintained in a 12:12 hours light dark cycle.

METHOD DETAILS

Clinical and laboratory parameters

Completed medical history and anthropometric variables were collected from all participants. In fasting conditions, a blood sample was provided. Fasting plasma glucose (FPG) and lipid profiles were measured by standard laboratory methods using an analyzer (CobasR 8000 c702, Roche Diagnostics, Basel, Switzerland). High-sensitivity C-reactive protein (hsCRP) levels were determined by immunoturbidimetric method (CobasR 8000 c702, Roche Diagnostics, Basel, Switzerland). Glycated hemoglobin (HbA1c) was determined by high performance liquid chromatography (ADAMRA1c HA-8180V, ARKRAY, Kyoto, Japan).

Body composition

Fat mass (FM), fat free mass (FFM) and their distribution was measured by a dual energy xray absorptiometry (DEXA, GE lunar, Madison, Wisconsin).

Dietary pattern

The dietary characteristics of the subjects in the IRONMET and INTESTINE cohorts were collected in a personal interview using a validated semi-quantitative food-frequency questionnaire (FFQ), including 93 different kinds of foods and beverages commonly consumed in Spain (available at: http://epinut.edu.umh.es/en/cfa-93-encv/). The FFQ is a Spanish version of the Harvard Questionnaire (Willett et al., 1985) which was modified and validated for the Mediterranean area of Spain (Vioque et al., 2013). Participants were asked how often on average they had consumed each food item during the previous year. Serving sizes were specified for each food item in the FFQ. The FFQ had nine possible responses, ranging from "never or < 1 per month" to "6 or more per day". Average daily nutrient intakes were obtained by multiplying the consumption frequency of each food item by the nutrient content in the specified portion/serving specified on the FFQ. The nutrient values were obtained from the food composition tables of the US Department of Agriculture (http://www.nal.usda.gov/ fnic/foodcomp), which includes data on practically all food items available in Spain and on a wide variety of ethnic foods, as well as other published sources for Spanish foods and portion sizes (Imma Palma et al., 2008).

Cognitive assessment

The Patient Health Questionnaire-9 (PHQ-9) is the depression module of the PRIME-MD diagnostic instrument for mental disorders (Spitzer et al., 1999). It is a self-administered questionnaire and consists of 9 items of depression symptoms plus a question about functional impairment. The PHQ-9 can be scored either as a depression severity rating (range 0-27 points) or with an algorithm based on the DSM-IV criteria (major and minor episode). It can also be interpreted using a cut-off point applied the symptom severity score. Scores of 10 to 14 represent a moderate symptom severity level, 15 to 19 represent moderately severe symptoms, and 20 to 27 severe depressive symptoms. Scores of 10 or more have an 88% sensitivity and specificity.

MRI acquisition and image pre-processing

All subjects were studied on a 1.5T Ingenia (Philips Healthcare, Best, The Netherlands) with eight channel head coils. As a part of a larger study protocol a multislice fluid attenuation inversion recovery (T2-FLAIR) with TR/TE/TI=6500/120/2200ms, flip angle 90°, in-plane resolution 0.78x0.78mm, slice thickness 5mm without gap and 20 axial slices was used to exclude pre-existing brain lesions.

MRI relaxometry was assessed by using a multi-echo gradient echo sequence with TR/1stTE/ΔTE=800/2.2/5ms, flip angle 80°, in-plane resolution2x2mm, slice thickness 5mm without gap and 20 axial slices. After acquisition, T2* and R2* maps were computed using Olea Sphere 3.0 (Olea Medical, La Ciotat, France) with Bayesian analysis algorithm. T2* maps were calculated by fitting the signal decay curve of the respective magnitude multiecho data and R2* maps were calculated as R2* = 1/T2*. In addition, a brain extraction tool was used to delete all non-brain tissues of calculated T2* and R2* maps. R2* were measured in s^{-1}.

Intrinsic-ignition framework

Image acquisition, pre-processing and phase synchronization for the fMRI study have been describe in detail elsewhere (Escrichs et al., 2021). We applied the Intrinsic-Ignition Framework (Deco and Kringelbach, 2017) to obtain the effect of naturally occurring activation events that reflect the capability of a given brain area to propagate activity to other brain areas. In brief, we transformed the BOLD time series to phase space by filtering the signals within the narrowband (0.04-0.07 Hz) and computed the Hilbert transform to obtain the phases of the signal between each pair of brain areas at each time point. Figure 4C shows the representation of the Hilbert BOLD phase for a brain area over time in the complex plane. Figure 4D shows the algorithm used to obtain the ignition value of each brain area evoked by an event within a set time window. The binary events were defined by transforming the time series into z-scores, $z_i(t)$, and fixing a threshold, θ. Then, a phase lock matrix $P_{jk}(t)$, was computed which describes the state of phase synchronization between brain areas j and k at time t as:

$$P_{jk}(t) = e^{-3\left|\varphi_j(t) - \varphi_k(t)\right|}$$

where $\varphi_j(t)$ and $\varphi_j(t)$ correspond to the phases of the BOLD time series for brain areas j and k at time t. Then, the integration was defined by measuring the length of largest connected component in the phase lock matrix $P_{jk}(t)$ and the value of integration was computed as the length of the connected component considered as an adjacent graph (*i.e.*, the largest subcomponent). Finally, for each brain area, we averaged across the events the integration evoked at each time t within the set time window. A complete description of the method can be consulted in Deco and Kringelbach (2017).

Extraction of fecal genomic DNA and whole-genome shotgun sequencing

Total DNA was extracted from frozen human stools using the QIAamp DNA mini stool kit (Qiagen, Courtaboeuf, France). Quantification of DNA was performed with a Qubit 3.0 fluorometer (Thermo Fisher Scientific, Carlsbad, CA, USA), and 1 ng of each sample (0.2 ng/μl) was used for shot gun library preparation for high-throughput sequencing, using the Nextera DNA Flex Library Prep kit (Illumina, San Diego, CA, USA) according to the manufacturers' protocol.

Sequencing was carried out on a NextSeq 500 sequencing system (Illumina) with 2 X 150-bp paired-end chemistry, at the facilities of the Sequencing and Bioinformatic Service of the FISABIO (Valencia, Spain). The obtained input fastq files were decompressed, filtered and 3· ends-trimmed by quality, using prinseq-lite-0.20.4 program (Schmieder and Edwards, 2011) and overlapping pairs were joined using FLASH-1.2.11 (Magoč and Salzberg, 2011). Fastq files were then converted into fast files, and human and mouse host reads were removed by mapping the reads against the GRCh38.p11, reference human genome (Dec 2013), and GRCm38.p6, reference mouse genome (Sept 2017), respectively, by using bowtie2-2.3.4.3 (Langmead and Salzberg, 2012) with end-to-end and very sensitive options. Next, functional analyses were carried out by assembling the non-host reads into contigs by MEGAHIT v1.1.2 (Li et al., 2015) and mapping those reads against the contigs with bowtie2. Reads that did not assemble were appended to the contigs. Next, the program Prodigal v2.6.342 (Hyatt et al., 2010) was used for predicting codifying regions. Functional annotation was carried out with HMMER (Durbin et al., 1998) against the Kyoto Encyclopedia of Genes and Genomes (KEGG) database, version 2016 (Kanehisa and Goto, 2000) to obtain the functional subcategory, route and annotation of the genes. The filtering of the best annotations and the assignment of the orf annotation to every read were carried out using the statistical package R 3.1.0 (R Development Core Team, 2013) which also was used to count the aligned reads and to add the category and its coverage, and finally to build abundance matrices. Taxonomic annotation, was implemented with Kaiju v1.6.2 (Menzel et al., 2016) on the human and mouse-free reads. Addition of lineage information was added, counting of taxa and generation of an abundance matrix for all samples were performed using the package R.

Jejunal stranded RNA sequencing

Intestinal epithelium from jejunum was collected during gastric by-pass surgery in RNAlater (Thermo Fisher Scientific), to preserve RNA integrity. Then, samples were immediately transported to the laboratory. The handling of tissue was carried out under strictly aseptic conditions and stored at -80°C. RNA purification was performed using RNeasy-Tissue Mini-Kit (QIAgen). Total RNA was quantified by Qubit RNA BR Assay kit (Thermo Fisher Scientific) and the integrity was checked by using the RNA Kit (15NT) on 5300 Fragment Analyzer System (Agilent). The RNASeq libraries were prepared with Illumina TruSeq Stranded Total RNA Sample Preparation kit following the manufacturer's recommendations with some modifications. Briefly, in function of availability 100-500ng of total RNA was rRNA depleted using the RiboZero Magnetic Gold Kit and fragmented by divalent cations. The strand specificity was achieved during the second strand synthesis performed in the presence of dUTP. The cDNA was adenylated and ligated to Illumina platform compatible IDT adaptors with unique dual indexes with unique molecular identifiers (Integrated DNA Technologies), for paired end sequencing. The ligation products were enriched with 15 PCR cycles and the final library was validated on an Agilent 2100 Bioanalyzer with the DNA 7500 assay (Agilent). The libraries were sequenced on NovaSeq 6000 (Illumina) in a

fraction of sequencing flow cell with a read length of 2x101bp following the manufacturer's protocol for dual indexing. Image analysis, base calling and quality scoring of the run were processed using the manufacturer's software Real Time Analysis (RTA v3.4.4) and followed by generation of FASTQ sequence files. RNA-seq reads were mapped against human reference genome (GRCh38) using STAR software version 2.5.3a (Dobin et al., 2013) with ENCODE parameters. Genes were quantified using RSEM version 1.3.0 (Li and Dewey, 2011) with default parameters and using the annotation file from GENCODE version 29.

Metabolomics analyses

HPCL-ESI-MS/MS metabolomics analyses (IRONMET, IMAGEOMICS)

For non-targeted metabolomics analysis, metabolites were extracted from plasma and fecal samples with methanol (containing phenylalanine-C13 as an internal standard) according to previously described methods (Wikoff et al., 2008). Briefly, for plasma samples 30μl of cold methanol were added to 10 μl of each sample, vortexed for 1 minute and incubated for one hour at −20 °C. For fecal samples, the content of a 1.2 ml tube of Lysing Matrix E (MP biomedicals) and 600 μl of cold methanol were added to 10mg of sample. Samples were homogenized using FastPrep-24 (MP biomedicals) and were incubated overnight in a rocker at 4°C. Then, all samples were centrifuged for three minutes at 12.000g, the supernatant was recovered and filtered with a 0.2 μm Eppendorf filter. Two μL of the extracted sample were applied onto a reversed-phase column (Zorbax SB-Aq 1.8 μm 2.1 x 50 mm; Agilent Technologies) equipped with a precolumn (Zorbax-SB-C8 Rapid Resolution Cartridge 2.1 x 30 mm 3.5 μm; Agilent Technologies) with a column temperature of 60°C. The flow rate was 0.6 mL/min. Solvent A was composed of water containing 0.2% acetic acid and solvent B was composed of methanol 0.2% acetic acid. The gradient started at 2% B and increased to 98% B in 13 min and held at 98% B for 6 min. Post-time was established in 5 min.

Data were collected in positive and negative electrospray modes time of flight operated in full-scan mode at 50–3000 m/z in an extended dynamic range (2 GHz), using N2 as the nebulizer gas (5 L/min, 350°C). The capillary voltage was 3500 V with a scan rate of 1 scan/s. The ESI source used a separate nebulizer for the continuous, low-level (10 L/min) introduction of reference mass compounds 121.050873 and 922.009798, which were used for continuous, online mass calibration. MassHunter Data Analysis Software (Agilent Technologies, Barcelona, Spain) was used to collect the results, and MassHunter Qualitative Analysis Software (Agilent Technologies, Barcelona, Spain) to obtain the molecular features of the samples, representing different, co-migrating ionic species of a given molecular entity using the Molecular Feature Extractor algorithm (Agilent Technologies, Barcelona, Spain). We selected samples with a minimum of 2 ions. Multiple charge states were forbidden. Compounds from different samples were aligned using a retention time window of 0.1% ± 0.25 minutes and a mass window of 20.0 ppm ±2.0 mDa. We selected only those present in at least 50% of the samples of one group and corrected for individual bias.

^{1}H-NMR Metabolomics analyses (IRONMET)

Plasma samples were thawed at room temperature. For each sample, 400 μL of plasma were combined with 200 μL of phosphate buffer ((9%w/V NaCl, 100% D_2O) that contained 10mM of 3-trimethylsilyl-1-[2,2,3,3-2H4] (TSP). Samples were mixed with the use of a vortex and centrifuged (10.000 x g) for 10 min. Then, a 550 μL aliquot was transferred into a 5 mm NMR tube prior to NMR analysis. ^{1}H spectra of low molecular weight metabolites were performed using a CPMG sequence (RD–90°–[t–180°– t]$_n$–ACQ-FID) with spin-echo delay of 400 μs (for a total T2 filter of 210 ms) allowing an efficient attenuation of the lipid NMR signals. The CPMG sequence generates spectra edited by T2 relaxation times, reducing broad resonances from high molecular weight compounds facilitating the observation of low molecular weight metabolites. The total acquisition time was 2.73 s with a RD of 2s and the 90° pulse length was automatically calibrated for each sample at around 11.1 μs. For each sample, 8 dummy scans were followed by 256 scans and collected in 64-K points over a spectral width of 20 ppm. TSP was used a general reference for NMR samples because it does not introduce any additional signals apart from the sharp methylsilyl resonance at 0 ppm. In addition, a high concentration of TSP was used to release low-molecular weight metabolites with high affinity for serum proteins by binding competition with TSP.

For fecal samples, 15-20 mg of dried fecal matter was is placed in a 2 ml Eppendorf tube. Then, 500 μL of 0.05 M PBS buffer in H_2O (pH=7.3) was added and vortexed vigorously, frozen and thawed twice and centrifuged (21000 g, 15 min, 4°C) to obtain a clear fecal water over the precipitated stool. From the upper layer, 200 μL of prepared fecal water was placed in appropriate 2 ml Eppendorf tube and then, 400 μL of 0.05M PBS buffer in D_2O (pH=7.2, TSP 0.7mM) was added. The sample was vigorously vortexed and sonicated until complete homogenization and the mixture (clear dispersion), if necessary, was centrifuged again (14000 rpm around 14000 g, 5 min, 4°C). For NMR measurement the clear upper phase was placed into a 5mm o.d. NMR tube. One dimensional ^{1}H pulse experiments were carried out using the NOESY-presaturation sequence [recycle delay (RD)-90°–t_1–90°–t_m–90° acquire (ACQ) free induction decay (FID)] to suppress the residual water peak. For each sample, 8 dummy scans were followed by 256 scans and collected in 64-K points over a spectral width of 20 ppm.

All ^{1}H-NMR spectra were recorded at 300 K on an Avance III 600 spectrometer (Bruker, Germany) operating at a proton frequency of 600.20 MHz using a 5 mm PABBO gradient probe and automatic sample changer with a cooling rack at 4°C.

Proline supplementation mice experiment

Unpredictable Chronic Mild Stress procedure (UCMS)

Three days after the beginning of the exposure to the different diets and to l-proline the UCMS protocol started (similar to the one previously published by (Farley et al., 2010)). During the dark part of the cycle stressors were applied twice a day for a maximum of 3 h/stressor (and a minimum of 1 h resting in between stressors) in a randomized order. Mice were exposed to tilted cages (45°), wet bedding (150 ml of water/100 g sawdust bedding), paired housing, crowding, home cage bedding with the smell of an

unknown mouse, unpredictable illumination, housed in a cage with no bedding and with 2 cm depth of water, and tail suspension test (only once). Stressors during the light part of the cycle (12 h) included tilted cages, wet bedding and bedding with the smell of unknown mouse. Exposure to the UCMS protocol lasted for 6 weeks. Body weight and fur conditions were regularly checked. Control mice were left undisturbed in a separate room, with the exception of the weekly measurements of body weight and the sucrose intake (individualized) and tail suspension test evaluation (performed on the same days as the UCMS mice). Mice were sacrificed 12 h after the exposure to the last stressor, 43 days after the beginning of the UCMS protocol. Plasma samples, cecum and fecal pellets were obtained.

Sucrose consumption test

To evaluate the development of an anhedonic-like behavior. Previous habituation to sucrose consumption, sucrose intake (4%, 2 h) measurement were performed on both, control and UCMS mice, 41 days after the beginning of the UCMS protocol by using calibrated pipettes.

Tail suspension test

The tail suspension test was performed as previously reported (Mato et al., 2007). Animals were individually suspended by the tail using adhesive tape (distance from tip of tail was 2 cm). Mice were suspended for 6 min. Immobility time (depressive-like behavior) was evaluated on the last 4 min of the test. Mice were exposed to the tail suspension test 40 days after the beginning of the UCMS protocol. Both, control and UCMS mice, were exposed to the test the same day.

LBP and zonulin measurements

Mice serum LBP (HK205-02, LBP mouse ELISA kit, Hycult Biotech, PA, USA) were measured using commercial kits according to manufacturer's instructions with intra- and inter-assay coefficients of variation <8%. Serum LBP (HK315-02, human LBP ELISA kit, HyCult Biotechnology, Huden, the Netherlands) and zonulin (K 5601, IDK Zonulin (Serum) ELISA, Immunodiagnostik AG, Germany) in the IRONMET cohort were also measured using commercial kits according to manufacturer's instructions.

Animals fecal microbiome transplantation (FMT) experiment

Experimental design

Mice were given *ad libitum* cocktail of antibiotics during 14 days in drinking water to deplete gut microbiota. Antibiotic cocktail consisted of ampicillin (1 g/L), metronidazole (1 g/L), vancomycin (400 mg/L), ciprofloxacin HCl (250 mg/L) and imipenem (250 mg/L). After 14 days of antibiotic intake animals were subjected to a 72 hours wash out and then colonized via daily oral gavage of donor microbiota (200 μL) for 3 days. Animals were orally gavaged with saline (Control, n=10) or fecal material from patients with a range of PHQ-9 scores (FMT, n=20). Booster inoculations were given twice weekly to throughout the study to reinforce donor microbiota phenotype. Animals were exposed to a fear conditioning test with nociception assessed by the hot plate test to ensure specificity. At the end of the study, animals were consecutively sacrificed and the brains were quickly removed and the medial prefrontal cortex was dissected according to the atlas of stereotaxic coordinates of mouse brain (Paxinos and Franklin, 1997). Brain tissues were then frozen by immersion in 2-methylbutane surrounded by dry ice, and stored at -80°C. The cecum was removed, weighed and stored, and the feces collected and stored at −80 °C for further microbiota analysis. Fecal microbiota composition from mice was analyzed following the same procedures as for humans.

Emotional testing in mice

Fear conditioning was conducted as described previously with some modifications (Saravia et al., 2019). Mice were individually placed in a shuttle chamber (LE918, Panlab, Barcelona) surrounded by a sound-attenuating cabinet. The chamber floor was formed by parallel stainless-steel bars connected to a scrambled shock generator. On the training day, mice were habituated to the chamber during 180 s before the exposure to an acute beeping 30 s sound (80 dB). Each animal received an unconditioned stimulus (US) (0.6 mA footshock during 2 s) paired with the end of the sound (conditioned stimulus, CS). After the shock, the animal remained for 60 s in the shuttle chamber. To evaluate cued fear conditioning, mice were re-exposed to the CS in a novel environment (a wide white cylinder in the chamber) 24 h after the conditioning session. Mice were allowed to adapt for 180 s to the new environment which was followed by 30 s of the sound used in the training day. After the last sound trial, mice remained in the cylinder for 60 s. Fear memory was assessed as the percentage of time that mice spent freezing during the session. Freezing response, a rodent's natural response to fear, was evaluated by direct observation and defined as complete lack of movement, except for respiration for more than 1 s. The procedure was performed between 8.00 and 12.00 h in an experimental room different to the housing room.

Study of gene expression in the mice prefrontal cortex

RNA quality control performed using the RNA 6000 Nano chip (Agilent) on an Agilent Bioanalyzer 2100 obtaining RIN values between 8.7 - 9.8. Libraries were prepared from 500 ng of total RNA using the TruSeq stranded mRNA library preparation kit (Illumina, #20020594) with TruSeq RNA Single Indexes (Illumina, #20020492 and #20020493) according to the manufacturer's instruction reducing the RNA fragmentation time to 4.5 minutes. Prepared libraries were analyzed on a DNA 1000 chip on the Bioanalyzer and quantified using the KAPA Library Quantification Kit (Roche, #07960204001) on an ABI 7900HT qPCR instrument (Applied Biosystems). Sequencing was performed with 2x50 bp paired-end reads on a HiSeq 2500 (Illumina) using HiSeq v4 sequencing chemistry. Raw sequencing reads in the fastq files were mapped with STAR version 2.5.3a (Dobin et al., 2013) to the Gencode release 17 based on the GRCm38.p6 reference genome and the corresponding GTF file. The table of counts was obtained with FeatureCounts function in the package subread, version 1.5.1 (Liao et al., 2014). Genes having less than 10 counts in at least 5 samples were excluded from the analysis.

Drosophila melanogaster experiments

Bacterial strains and growth

The bacterial strains *Lactobacillus Plantarum* (DSM 2601) and *Enterobacter cloacae* (DSM 6234) were obtained from DSMZ, German Collection of Microorganisms and Cell Cultures GmbH (Germany). *L. Plantarum* strains were cultured in MRS modified broth (Koyle et al., 2016) and *E. Cloacae* strains were cultured in LB broth (Sigma) in 14-mL culture tubes at 30 °C, with agitation, overnight.

Inoculated tubes for mono-associated flies were created by separately culturing the bacterium of interest overnight in the corresponding media, washing them in phosphate-buffered saline (PBS), normalizing to an optical density at 600 nm (OD600) of 0.1 in PBS as described in Koyle et al. (2016) and inoculating 35 μl or 300 μl of normalized culture in to 15 or 45 mmm diameter vials respectively, on top of the sterile diet with a sterile Whatman filter paper.

Generation of axenic and mono-associated flies

To generate axenic flies >17 hours embryos were collected in apple juice agar plates and sterilized with 50% bleach during 5 minutes, rinsed twice in sterile water for 5 min and placed on sterile standard food supplemented with antibiotics (50 μg ampicillin, 50 μg kanamycin, 50 μg tetracycline and 15 μg erythromycin per liter of fly food) in 45 mm diameter vials with a sterile Whatman paper. Flies were maintained for a minimum of 2 generations in antibiotic media to clear possible *Wolbachia* infection. Absence of *Wolbachia* was verified by PCR using *Wolbachia*-specific primers, as described previously (Merkling and Van Rij, 2015). After Wolbachia clearance, conventionally reared stocks were used to regenerate axenic stocks regularly exclusively performing the egg bleaching treatment.

For bacterial mono-association at the larval stage, sterilized eggs were transferred to 45 mm vials with sterilized diet and 24 hours later tubes were inoculated the corresponding bacterial load (see bacterial strains and growth section) and reared until adulthood. The experimental germ-free condition was obtained by inoculating the corresponding amount of sterile PBS to the fly food.

For bacterial mono-association at the adult stage, sterilized embryos were raised in standard food with antibiotics as described above until day one of adulthood, then flies were transferred into 15 mm diameter antibiotic-free fly food inoculated vials with the corresponding bacterial load. Flies were kept in the vial until the experimental test.

Adults were tested for axenicity or the correct bacterial mono-association previous to the experiment plating the fly lysate on different bacterial culture media. All these procedures were performed under the hood, with sterile material and under sterile conditions.

Mechanical stress treatment

Mechanical stress treatment was performed with a few modifications from the previously described protocol (Ries et al., 2017). According to the experimental condition, male or female one day old adults were collected and placed in the corresponding fly food vials in groups of 25 to 30 flies. After two days, tubes were either placed on a stable surface (unstressed group) or on top of a vibration device (stressed group). Stressed and unstressed flies always came from the same culture vials; assignment was random. In this protocol mechanical-stress was induced by a shaker (Labinco-LD450) controlled by an Arduino Uno chip (Arduino), that permitted to control rotational speed and the duration of the on/off vibration protocol duration. The shaker controller protocol was applying the following parameters: the angular velocity control was set at 105 for 20 s followed by a pause of 10 s. The 20 s/10 s schema was repeated for 15 min followed by a 30 min break, 16 cycles were applied per day corresponding to 12 hours a day, from 6AM to 6PM. The fifth day of mechanical stress treatment, stressed and unstressed flies were tested.

Gap climbing assay

One day old male flies got their wings clipped and were placed back for recovery on standard cornmeal medium for 16–24 h. Gap climbing assay was performed as described by Pick and Strauss (2005) and Ries et al. (2017). During the Pretest, flies were tested individually in the climbing paradigm on a 4 mm wide, 10 mm high and 35 mm long catwalk made of black polycarbonate with an insurmountable 4.5 mm wide, 6 mm deep gap in the center. The catwalk was situated on a circular island of 28 mm diameter surrounded by water and a cylindrical plain white shield. Positive climbing attempts were visually identified when the typical 'leg-over-head behavior' was observed. After ten approaches to the gap, the percentage of positive climbing attempts was registered. After 5 days of either vibrational stress or control treatment the flies were retested in the climbing paradigm under the same conditions (Test). To avoid contamination with non-desired bacteria, the "Presets" was avoided with mono-associated or axenic flies and only the "Test" was performed. All gap climbing tests were performed within the same time of the day (9 to 12 AM).

Stop for sweet paradigm (SFS)

Stop for sweet paradigm was performed modifying the previously described by Ries et al. (2017). Virgin female flies were collected and separated into stress or unstressed treatment groups as described previously. Previous to the test, the flies were starved for 36, 48, or 60 hours by transferring the flies to a new vial with 0,4% agar depending on the genotype. After 5 days of treatment flies were individually tested in the stop-for sweet paradigm (the test was always performed between 6 and 8 PM).

The starvation time applied to each genotype was established according to the maximum starvation time where 90% of the flies of the corresponding control or axenic condition survived. Lethality was evaluated every 12 hours. For all tested conditions, with the exception of *Slc6a20RNAi x UAs-Dcr2; elav-GAL4* 12 hours prolongation in the starvation time led to a lethality of more than 60% of the flies. Mono-associations with *E. Cloacae* considerably decreased resistance to starvation leading to premature dead, therefore the number of flies tested in the stop for sweet paradigm for this condition was very low or could not be performed.

Stop for sweet chambers were assembled with a laser cut transparent polycarbonate sheet (115 x 115 x 3 mm, round shaped borders (radius=15), with two parallel rectangular apertures in the center of 55 × 20 mm speared by 15 mm, CanMake). The polycarbonate sheet was placed inside the cover of a 120x120 mm square shaped petri dish plate (Monolab), the petri dish bottom was placed on top resembling a sandwich, creating two chambers of 55 × 20 x 3 mm. Flies were introduced into the cambers throughout a 1,5 mm diameter hole

created in the petri dish bottom. Before the experiment started, a cut of 120x120 filter paper (VWR, 600 medium filtration rate, particle retention10-20μl) was placed in the inner part of the petri dish cover and secured by tape, a 5 mm wide trace of glycerol (99.5%, Sigma) saturated with powdered sucrose was painted at the midline of each camber with a fine paintbrush, and the montage of the camber was assembled as described above. A fly was placed in each chamber with the aspirator. The two flies were shaken down to the bottom of their chambers to induce negative geotaxis, and the flies were instinctively climbing up crossing the line of sweet tasting glycerol pained on the filter paper. To favor the flies to walk on the paper rather than on the lid, the chamber was held over vertical (110°–120°). For 10 consecutive trials, it was observed if the fly overrun the sweet tasting glycerol line or stopped to eat and the percentage of stops was annotated. Flies that were not able to climb were discarded from the experiment.

Spontaneous locomotor activity

Tracking arenas were created with modified lids of 60 mm petri dishes, with a height of 4 mm to allow flies to freely walk but not to jump or fly. Flies were transferred to the arena using an aspirator and were allowed to acclimatize for 5 min. Next, 5 min videos (24 fps) were recorded using a Logitech C525 webcam positioned above the center of the arena. Locomotion was tracked using the semi-automatic machine-vision program Ctrax (Version 0.5.18) (Branson et al., 2009). Distances within the videos were calibrated based on a known measure. Ctrax output files were further analyzed in Excel to calculate total distance and velocity while in motion (flies were considered in motion where the distance travelled within two frames was bigger than 0,1 mm).

QUANTIFICATION AND STATISTICAL ANALYSIS

Clinical variables

First, normal distribution and homogeneity of variances were tested using the Kolmogorov-Smirnov and the Levene's tests, respectively. Results are expressed as number and frequencies for categorical variables, mean and standard deviation (SD) for normal distributed continuous variables and median and interquartile range [IQ] for non-normal distributed continuous variables. To determine differences between study groups, we used χ^2 for categorical variables, unpaired Student's t test in normal quantitative and Mann-Whitney U test for non-normal quantitative variables. Spearman or Pearson analysis was used to determine the correlation between quantitative variables. Theses statistical analyses were performed with SPSS, version 19 (SPSS, Chicago, IL). Statistics can be found in the figures and legends.

Metagenomics analyses

To take into account the compositional structure of the microbiome data and rule out possible spurious associations, raw counts were transformed using a centered log-ratio (clr) transformation as implemented in the ''ALDEx2'' R package (Fernandes et al., 2014). It first uses a Dirichlet-multinomial model to infer abundance from read counts and then applies a clr transformation to each instance. We used 128 Dirichlet Monte Carlo instances in the aldex.clr function. Bacterial species and functions associated with the PHQ-9 scores were identified using robust linear regression models as implemented in the Limma R package (Ritchie et al., 2015), adjusting for age, body mass index, sex, education years, antidepressant and anxiety medication. Taxa and bacterial functions were previously filtered so that only those with more than 10 reads in at least five samples were selected. The p values were adjusted for multiple comparisons using a Sequential Goodness of Fit (Carvajal-Rodríguez et al., 2009) as implemented in the ''SGoF'' R package. Unlike FDR methods, which decrease their statistical power as the number of test increases, SGoF methods increase their power with increasing number of tests. SGoF has proven to behave particularly better than FDR methods with high number of tests and low sample size, which is the case of omics large datasets. Statistical significance was set at padj<0.1.

Metabolomics and whole-brain functional dynamics analysis

Metabolomics data were first normalized using a probabilistic quotient normalization. Metabolomics and whole-brain functional dynamics data were analyzed using machine learning (ML) methods. In particular, we adopted an all-relevant ML variable selection strategy applying a multiple random forest (RF)-based method as implemented in the Boruta algorithm (Kursa and Rudnicki, 2010), It has been recently proposed as one of the two best-performing variable selection methods making use of RF for high-dimensional omics datasets (Degenhardt et al., 2019). The Boruta algorithm is a wrapper algorithm that performs feature selection based on the learning performance of the model (Kursa and Rudnicki, 2010). It performs variables selection in three steps: a) Randomization, which is based on creating a duplicate copy of the original features randomly permutates across the observations; b) Model building, based on RF with the extended data set to compute the normalized permutation variable importance (VIM) scores; c) Statistical testing, to find those relevant features with a VIM higher than the best randomly permutated variable using a Bonferroni corrected two-tailed binomial test; and d) Iteration, until the status of all features is decided. We run the Boruta algorithm with 500 iterations, a confidence level cut-off of 0.005 for the Bonferroni adjusted p values, 5000 trees to grow the forest (ntree), and a number of features randomly sampled at each split given by the rounded down number of features/3 (the mtry recommended for regression). Pathway over-representation analysis was performed mapping metabolites that were significantly associated with the PHQ-9 in the discovery cohort to the KEGG, Reactome, INOH and HumanCyc databases included in the ConsensusPathDB (Kamburov et al., 2013).

RNA-seq analysis

Differential expression gene analyses were performed on gene counts using the ''limma'' R package (Ritchie et al., 2015). First, low expressed genes were filtered, so that only gene with more than 10 reads in at least 2 samples were selected. After filtering, 15,144

genes out of 22,204 were retained for subsequent analyses. RNA-seq data were then normalized for RNA composition using the trimmed mean of M-value (TMM) as implemented in edgeR package (Robinson et al., 2010). Normalized counts were then converted to $\log_2$ count per million (logCPM) with associated precision weights to account for variations in precision between different observations using the "voom" function with donor's age, BMI, sex, education years, antidepressant and anxiety medication, and kcal intake as covariates. A robust linear regression model adjusted the previous covariates was then fitted to the data using the "lmFit" function with the option method = "robust", to limit the influence of outlying samples. Finally, an empirical Bayes method was applied to borrow information between genes with the "eBayes" function. Over-representation analyses were performed by mapping differentially expressed genes into the Reactome, KEGG, and DisGeNET databases. Pathway significance was assessed using a hypergeometric test and a Storey procedure (*q*-values) was applied for multiple testing correction. Statistical significance was set at qval<0.1. For the FMT study, differentially expressed genes were also mapped to the Search Tool for Retrieval of Interacting Proteins/Genes (STRING) database (which integrates known and predicted protein/gene interactions) to predict functional gene-gene interaction networks (Szklarczyk et al., 2019). Then, functional local clusters in the interaction network were determined using a Markov Cluster algorithm (MCL) with an inflation parameter = 3. Active interacting sources including text mining, experiments, databases, co-expression, and co-occurrence and an interaction score > 0.4 were used to construct the interaction networks.

In the animal studies, each experimental condition was repeated a minimum of 3 times. Significance was calculated using non-paramedical Kruskal-Wallis test for multiple comparisons with Prism (Version. 9.3.1).

The statistical parameters can also be found in the figures and figure legends.